Journal of Engineering Mathematics (2006) 55: 9–39
DOI 10.1007/s10665-005-9022-1


# Hydrodynamic interaction of axial turbomachine cascades

V.E. SAREN[1], N.M. SAVIN[1], S.A. SMIRNOV[1], V.G. KRUPA[1] and V.A. YUDIN[2]
[1] *Central Institute of Aviation Motors, 2, Aviamotornaja st., Moscow 111116, Russia (saren@ciam.ru)*
[2] *Lavrentyev Institute of Hydrodynamics, 15, pr. Ac. Lavrentyeva., Novosibirsk 630090, Russia*

Received 14 March 2004; accepted in revised form 19 September 2005 / Published online: 3 January 2006

**Abstract.** Hydrodynamic interaction of mutually moving airfoil cascades is investigated. It is shown that the semi-empirical theory of potential-vortical interaction of two mutually moving cascades in incompressible flow allows one to describe correctly the features of their mutual effect for various gaps between cascades and relations of their pitches. Application of the above theory to a flow around three cascades of the stator-rotor-stator type allows to determine the basic mechanism of the stators' mutual shift effects (clocking effects). To close the theory regarding the vortical interaction of cascades, a semi-empirical model of turbulent diffusion in a non-uniform flow of the periodic vortices descending from airfoils is proposed. Theoretical results are compared with data from numerical and physical experiments. Comparison with results of numerical modeling is based on the solution of the Reynolds equations for a viscous gas closed by the ($q$-$\omega$) model of turbulence. Results published here and elsewhere are used for comparison with measurement data.

**Key words:** cascade of airfoils, clocking effect, periodic vortex wakes, rotor-stator interaction

## 1. Introduction

Rotor-stator interaction is one of the most topical and challenging problems of turbomachine aerodynamics. The enormous experience accumulated during the development of gas-turbine engines and power plants proves to be insufficient for estimating the pressure pulsations at the design stage, causing blade vibrations, radiated noise, and gas-dynamic losses in promising compressors and turbines designed for high-power characteristics of stages. This has given rise to numerous research activities involving mainly by numerical methods.

Analytical and semi-analytical methods, whose development is dealt with in the present work, are based on more specific flow models. They enable one to obtain solutions that clearly describe the qualitative features of blade-rows interaction within the framework of the accepted assumptions. Such solutions, which are necessary both for setting up experiments and for engineering estimates, successfully supplement numerical methods towards the solution of more general problems. The present paper contains results obtained by the authors in a theoretical study of the flow of mutually moving cascades. For comparison and illustration of results, both the experimental data and the numerical solutions obtained by authors are used.

The basic part of the paper is devoted to the development of the theory of potential-vortical interaction of cascades in incompressible flow [1–4]. The unsteady velocity disturbances caused by two mutually moving cascades are assumed to be potential almost everywhere in the flow, and turbulent vortex wakes of the cascade located upstream are described by the self-similar theory. The obtained solution has allowed us to estimate theoretically for the first time the effect of unsteady interaction of cascades on time-averaged aerodynamic loadings and to describe correctly the effect of a gap between cascades on a level and character of

unsteady loadings. A problem formulation within the framework of potential-vortex interaction, which is now the most general available, is presented in Section 3.

An illustrative example of a successful application of the potential-vortical interaction theory is the detection and subsequent explanation of the essential effect of the stators' mutual shift on an unsteady rotor flow in a system of stator-rotor-stator rows. The latter is known as the clocking effect. It follows from these results that for an equal (or multiple) number of stator vanes, the optimization of their mutual circumferential position is an efficient means of reducing pressure pulsations caused by rotor-stator interaction. A direct experimental test of the clocking effect was executed for the first time during the transonic and subsonic stages of an axial compressor [5, 6]. Similar experiments and a numerical analysis have been executed for turbine stages in [7–9]. Further experimental and numerical studies were performed for a subsonic model stage of the axial compressor[1] [10–13]. The practical importance of this problem has led to a continuation of the investigations devoted to the clocking effect (see, for example, [14, 15]).

The theoretical fundamentals of the clocking effect are stated in Section 4, where comparisons with data obtained on a large-size experimental set-up[2] [16, 17] and with results of a numerical solution of the Reynolds equations closed by the ($q$-$\omega$) model of turbulence are also presented. The numerical algorithm is described in Section 4.3.

One of the results of the numerical and experimental studies reported here consists of the fact that the additional gas-dynamic losses caused by rotor-stator interaction are due to the dissipation of periodic vortices blown off by the flow and, according to Thomson's theorem, arising behind blade rows. Classical modeling of the contact discontinuity line identified in the flow of vortices, as well as the model of their viscous diffusion used in Section 3, does not correspond to the observed structure of the wakes [18]. In Section 5, a semi-empirical model of turbulent diffusion of free vortices, taking into account velocity distortion of their blow-off in the wake flow behind airfoils, is proposed. Comparisons with experiment and results of our numerical modeling show that the proposed solution can be used for the analysis of the structure of periodic vortical wakes and, in particular, allows one to close the theory of potential-vortical interaction of cascades by a more adequate physical model.

## 2. Periodic flow in a stage of an axial turbomachine

The stage of an axial turbomachine represents a set of rotating (rotor) and motionless (stator) blade rows in the annular channel with some axial gap $\Delta$. At the design stage the flow upstream of each row is usually assumed to be averaged over a circle. In this case, the relative flow in a frame of reference connected with the given row is stationary and is defined completely by the row geometry and flow conditions at the inlet. Actually, for finite values of $\Delta$ in each reference frame, rotating or motionless, the flow is periodic in time $t$ with the basic frequency of the next row blade passing.

Let $(r, \varphi, x)$ and $(r, \varphi_0, x)$ be the cylindrical coordinates connected with a rotor and stator, respectively, and $\Pi$ be some flow parameter (velocity or pressure) evaluated in one of the reference frames. At constant rotor rotation speed $\Omega_0$, a turn of any of the rows through an angle $\Delta\varphi$ or $\Delta\varphi_0$ between respective lines of the next blades is equivalent to a displacement in time of $\Delta\varphi/\Omega_0$ for the rotor reference frame and of $\Delta\varphi_0/\Omega_0$ for the stator reference frame.

[1]Financial support was provided by the Russian Foundation for Basic Research, Grant No. 96-01-01847, and CRDF, Grant No. 1-195

[2]Financial support was provided by the Russian Foundation for Basic Research, Grant No. 93-013-16653, and ISTC, Projects Nos. 672-98, 672,2.

Here the angles $\varphi$ and $\varphi_0$ are assumed to be counted up to a side opposite to rotor rotation, and $\varphi = \varphi_0$ at the initial moment of time $t = 0$. This implies

$$\begin{aligned} &\Pi(r, \varphi, x, t + \Delta\varphi_0/\Omega_0) = \Pi(r, \varphi, x, t); \quad \Pi(r, \varphi + \Delta\varphi, x, t) = \Pi(r, \varphi, x, t - \Delta\varphi/\Omega_0), \\ &\Pi(r, \varphi_0, x, t + \Delta\varphi/\Omega_0) = \Pi(r, \varphi_0, x, t); \; \Pi(r, \varphi_0 + \Delta\varphi_0, x, t) = \Pi(x, r, \varphi_0, t + \Delta\varphi_0/\Omega_0), \end{aligned} \tag{1}$$

where the coordinates $\varphi$ and $\varphi_0$ are connected by a ratio

$$\varphi = \varphi_0 + \Omega_0 t.$$

The common notation has been related here for the same physical quantity $\Pi$ in the moving and fixed frames of reference, which does not give rise to any computational difficulties under a one-to-one correspondence of the explicitly given arguments.

From (1) it is easy to conclude that any flow parameter in a stage of an axial turbomachine can be represented by the following Fourier series

$$\begin{aligned} \Pi(r, \varphi, x, t) &= \sum_k \sum_l \Pi_{kl}(r, x) \cdot \mathrm{e}^{\mathrm{i}2\pi l \varphi/\Delta\varphi} \cdot \mathrm{e}^{\mathrm{j}2\pi k \varphi/\Delta\varphi_0} \cdot \mathrm{e}^{-\mathrm{j}2\pi k \Omega_0 t/\Delta\varphi_0}, \\ \Pi(r, \varphi_0, x, t) &= \sum_k \sum_l \Pi_{kl}(r, x) \cdot \mathrm{e}^{\mathrm{j}2\pi k \varphi_0/\Delta\varphi_0} \cdot \mathrm{e}^{\mathrm{i}2\pi l \varphi_0/\Delta\varphi} \mathrm{e}^{\mathrm{i}2\pi l \Omega_0 t/\Delta\varphi}. \end{aligned} \tag{2}$$

Here summation over the indices $k$ and $l$ is performed from $-\infty$ to $+\infty$, and the imaginary units subject to the condition of $\mathrm{i} \cdot \mathrm{j} \neq -1$ are denoted by i and j.

The coefficients of the expansions (2) can be determined by any of the two equalities

$$\begin{aligned} \Pi_{kl}(r, x) &= \frac{1}{\Delta\varphi_0 T_0} \int_0^{\Delta\varphi_0} \int_0^{T_0} \Pi(r, x, \varphi_0, t) \cdot \mathrm{e}^{-\mathrm{i}2\pi l t/T_0} \cdot \mathrm{e}^{-\mathrm{i}2\pi l \varphi_0/\Delta\varphi} \cdot \mathrm{e}^{-\mathrm{j}2\pi k \varphi_0/\Delta\varphi_0} \mathrm{d}t \mathrm{d}\varphi_0 \\ &= \frac{1}{\Delta\varphi T} \int_0^{\Delta\varphi} \int_0^{T} \Pi(r, x, \varphi, t) \cdot \mathrm{e}^{+\mathrm{j}2\pi k t/T} \cdot \mathrm{e}^{-\mathrm{j}2\pi k \varphi/\Delta\varphi_0} \cdot \mathrm{e}^{-\mathrm{i}2\pi l \varphi/\Delta\varphi} \mathrm{d}t \mathrm{d}\varphi, \end{aligned} \tag{3}$$

where $T_0 = \Delta\varphi/\Omega_0$ and $T = \Delta\varphi_0/\Omega_0$ are the time periods of change of the flow parameters in the stator and rotor reference frames, respectively.

Let

$$\begin{aligned} &\varphi = \bar{\varphi} + m \cdot \Delta\varphi, \quad m = 0, 1, \ldots, N_1 - 1, \\ &\varphi_0 = \bar{\varphi}_0 + m \cdot \Delta\varphi_0, \quad m = 0, 1, \ldots, N_2 - 1, \end{aligned}$$

where $\bar{\varphi}$ and $\bar{\varphi}_0$ are the angular coordinates of points on the original ($m = 0$) blades of a rotor and stator, respectively, and $N_1$ and $N_2$ are the respective numbers of blades in their total tangential period. Then (2) implies that each row of a stage induces a generally periodic flow containing one tangential period, namely $N_1$ or $N_2$ blades, respectively. Thus, the time-averaged linear aerodynamic loadings acting on a blade of a rotor ($R^{(1)}(r)$) or stator ($R^{(2)}(r)$), are equal to

$$R^{(1)}(r) = R_{00}^{(1)}(r) + \sum_{\substack{k \\ (k \neq 0)}} R_{k0}, \quad R^{(2)}(r) = R_{00}^{(2)}(r) + \sum_{\substack{l \\ (l \neq 0)}} R_{0l}, \tag{4}$$

where $R_{00}^{(1)}$ and $R_{00}^{(2)}$ are loadings on rotor and stator blades obtained by a tangential averaging of the relative flow upstream of each row, respectively, and $R_{k0}$ and $R_{0l}$ are the Fourier coefficients (2) obtained for aerodynamic loading on the rotor or stator blades.

Another important consequence of the representations (2) is the tangential non-uniformity of flow pulsations in a stage row. So, according to (2), for an isolated rotor the flow parameter $\Pi$ in an absolute frame of reference can be written as

$$\Pi(r, \varphi_0, x, t) = \sum_l \Pi_{0l}(r, x) \cdot e^{i2\pi l \varphi_0/\Delta\varphi} \cdot e^{i2\pi l t/T_0}.$$

This implies that the root-mean-square (rms) value of $\Pi$ pulsations over the period $T_0$,

$$\langle \Pi \rangle_t = \sqrt{\frac{1}{T_0} \int_0^{T_0} \Pi^2 dt} = \sqrt{\sum_l |\Pi_{0l}|^2},$$

does not depend on the tangential coordinate $\varphi_0$. For a stage rotor, it is easy to conclude from (2) that $\langle \Pi \rangle_t$ has the tangential period $\Delta\varphi_0$.

The above consequence means, in particular, that the difference in time-averaged static pressure for a stage rotor measured by motionless transducers on the housing or in a stream, appears to be non-uniform in the tangential direction. As was shown in [5, 6], this non-uniformity can be rather significant for highly loaded stages. On the other hand, it is clear that the tangential non-uniformity of time-averaged parameters of an absolute flow may be used as a measure of rotor-stator interaction.

It follows from (3) that, for the determination of any flow parameter concerning a rotor, it is sufficient to measure its change in time for a stator vane pitch $\Delta\varphi_0$. This property is widely used by the present authors when obtaining the experimental data for comparison with theoretical results.

Thus, the investigation of hydrodynamic interaction of rotors and stators in axial turbomachines leads to a need for investigating cascades of generally periodic flow, whose parameters may be represented in the form (2). Stationary gas-dynamic characteristics of both individual rows and stages as a whole are understood as a result of time-averaging of the series (2), and pressure pulsations on blades and in the stream are determined by the coefficients $\Pi_{kl}$ $(k, l = 0, \pm 1, \dots)$. The theoretical results presented in the following are for 2D flows when the dependence of the coefficients $\Pi_{kl}$ on radial coordinate $r$ is assumed to be insignificant.

## 3. Two mutually moving cascades of airfoils in incompressible flow

If the stream surfaces in a stage are assumed to be circular cylinders at each moment of time then, for a fixed radius $r$, the task is reduced to the calculation of the flow around two mutually moving cascades of airfoils in a uniform flow at an infinite distance upstream (Figure 1).

### 3.1. Mathematical formulation and solution

Let a continuous incompressible flow be realized on cascades of blades; the unsteady velocity disturbances can be assumed to be potential everywhere outside the zone of vortical wakes of the cascades. The required complex conjugate flow velocity may then be presented as

$$V_\Sigma(z, t) = V(z, t) + J(z) + J_1(z, t) + J_2(z, t). \tag{5}$$

Here $z = x + iy$ is the complex coordinate of a point, $V$ is an analytical function of $z$, $J$ is a piecewise continuous function determining the fluid velocity in the stationary vortical wakes of the cascades in the absence of their interaction, $J_1$ and $J_2$ are the velocities generated by periodic vortical wakes arising behind cascades 1 and 2, respectively, where cascade 1 is located upstream (Figures 1 and 2).

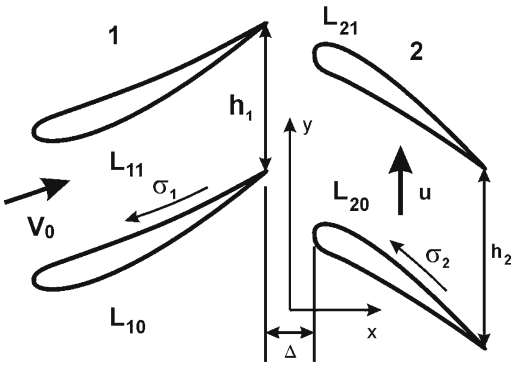


*Figure 1.* Mutually moving cascades of airfoils.

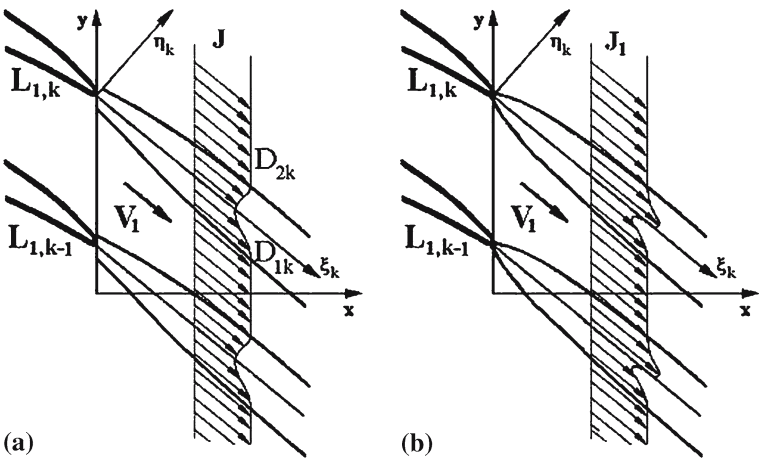


*Figure 2.* Flow velocity in steady (a) and unsteady (b) wakes of cascade 1.

If, for definiteness, it is assumed that cascade 2 moves with respect to cascade 1 at a speed $u = r\Omega_0$, then $V_\Sigma$ can be presented by a series such as (2), where it is necessary to put

$$\varphi_0/\Delta\varphi_0 = y_0/h_1, \quad \varphi/\Delta\varphi = y/h_2, \quad \Omega_0/\Delta\varphi_0 = -u/h_1, \quad \Omega_0/\Delta\varphi = -u/h_2, \quad y = y_0 - ut.$$

Here $h_1, h_2$ are the pitches of cascades 1 and 2, respectively.

A generally periodic analytical function $V(z,t)$ is expressed in terms of its boundary values $V_1$ and $V_2$ on cascades of blades 1 and 2 as Cauchy integrals as follows:

$$V(z,t) = \Phi_1[V_1, z] + \Phi_2[V_2, z] + V_\infty,$$

$$\Phi_\mu[V_\mu, z] = \frac{1}{H\mathrm{i}} \sum_{m=0}^{N_\mu - 1} \oint_{L_{\mu m}} V_\mu(\zeta, t) \frac{\mathrm{d}\zeta}{1 - \exp[2\pi(\zeta - z)/H]}, \quad \mu = 1, 2. \tag{6}$$

Here $L_{\mu m}$ is an airfoil of the $\mu$th cascade with number $m = 0, 1, \ldots, N_\mu - 1$ in the reference frame connected with the given cascade; $H = N_1 h_1 = N_2 h_2$ is the total spatial period of cascades; $V_\infty = \lim_{z \to -\infty} V$ is the absolute flow velocity at an infinite distance upstream of the cascades. The complex coordinate $z$ of a point in a moving coordinate system is related to the coordinate $z_0$ of the same point in the stator coordinate system by virtue of the equality $z = z_0 - \mathrm{i}ut$. Figure 1 shows a positive tracing of the profiles $L_{\mu m}$ and the arc coordinate $\sigma$ measured from the outlet edge.

Let the point $z$ tend to the points $z_0 \in L_{10}$ and $z \in L_{20}$ of the flow region. The limiting values $\Phi_1^-$ and $\Phi_2^-$ of the Cauchy integrals $\Phi_1$ and $\Phi_2$ are then determined by the Plemel–Sokhotzky formulas, and the regular terms in (6) are expanded into the series

$$\begin{aligned}\Phi_2[V_2, z_0] &= -\sum_{n=1}^{\infty} \sum_{m=0}^{N_2-1} \frac{1}{H\mathrm{i}} \oint_{L_{20}} V_2(\zeta + \mathrm{i}mh_2, t) \cdot \mathrm{e}^{-2\pi n(\zeta - \bar{z}_0)} \mathrm{d}\zeta \cdot \mathrm{e}^{-\mathrm{i}2\pi n(\omega t + \frac{m}{N_2})} \cdot \mathrm{e}^{-2\pi n\bar{\Delta}}, \\ \Phi_1[V_1, z] &= \sum_{n=0}^{\infty} \sum_{m=0}^{N_1-1} \frac{1}{H\mathrm{i}} \oint_{L_{10}} V_1(\zeta + \mathrm{i}mh_1, t) \cdot \mathrm{e}^{2\pi n(\zeta - \bar{z})} \mathrm{d}\zeta \cdot \mathrm{e}^{\mathrm{i}2\pi n(\omega t + \frac{m}{N_1})} \cdot \mathrm{e}^{-2\pi n\bar{\Delta}},\end{aligned} \tag{7}$$

where

$$\bar{z}_0 = \frac{z_0 + \Delta}{H}, \quad \bar{z} = \frac{z - \Delta}{H}, \quad \bar{\Delta} = \Delta / H, \quad \omega = u/H.$$

It follows from (7) that the boundary values $V_\mu$ $(\mu = 1, 2)$ of the function $V(z, t)$ on airfoils with numbers $m = 0, 1, 2, \ldots, N_\mu - 1$ may be presented in the form

$$V_\mu(z_\mu, t) = \sum_{n=0}^{\infty} \sum_{k=-n}^{n} U_{\mu kn}(z_\mu) \cdot \mathrm{e}^{\mathrm{j}2\pi k(\omega t + m\psi_\mu)} \cdot \mathrm{e}^{-2\pi n\bar{\Delta}}, \tag{8}$$

where

$z_1 = z_0 \in L_{10}$; $\quad z_2 = z \in L_{20}$; $\quad U_{\mu kn} = u_{\mu kn} + \mathrm{j}\ \mathrm{sqn}(k) \cdot v_{\mu kn}$; $\quad \psi_1 = 1/N_1$; $\quad \psi_2 = -1/N_2$. Indeed, for points $z_0 \in L_{10}$ and $z \in L_{20}$, the substitution of (8) in (6) and (7) results in the equalities

$$\sum_{n=0}^{\infty} \sum_{k=-n}^{n} \left\{ U_{\mu kn} - \Phi_\mu^-[U_{\mu kn}, z_\mu] \right\} \cdot \mathrm{e}^{\mathrm{j}2\pi k\omega t} \cdot \mathrm{e}^{-2\pi n\bar{\Delta}} = \sum_{n=0}^{\infty} \Pi_{\mu n}(z_\mu, t) \cdot \mathrm{e}^{-2\pi n\bar{\Delta}} + V_\infty, \tag{9}$$

$$\Pi_{1n} = -\sum_{m=-n}^{n-2} \sum_{k=k_1}^{n} \frac{1}{h_2\mathrm{i}} \oint_{L_{20}} U_2(\zeta, n + m - k, k) \cdot \mathrm{e}^{-2\pi(n-k)(\zeta - \bar{z}_0)} \mathrm{d}\zeta \cdot \mathrm{e}^{\mathrm{i}2\pi m\omega t} \cdot D_{2m}, \tag{10}$$

$$\Pi_{2n} = \sum_{m=-n}^{n} \sum_{k=k_2}^{n} \frac{1}{h_1\mathrm{i}} \oint_{L_{10}} U_1(\zeta, -n + m + k, k) \cdot \mathrm{e}^{2\pi(n-k)(\zeta - \bar{z})} \mathrm{d}\zeta \cdot \mathrm{e}^{-\mathrm{i}2\pi m\omega t} \cdot D_{1m},$$

where

$$U_\mu(\zeta, m, k) = u_{\mu mk}(\zeta) + \mathrm{i}\ \mathrm{sgn}(m) \cdot v_{\mu mk}(\zeta), \quad D_{\mu m} = \begin{cases} 1, & \frac{m}{N_\mu} = \left[\frac{m}{N_\mu}\right] \\ 0, & \frac{m}{N_\mu} \neq \left[\frac{m}{N_\mu}\right] \end{cases},$$

$$k_1 = \left[\frac{n + m + 1}{2}\right], \quad k_2 = \left[\frac{n - m + 1}{2}\right], \quad \mu = 1, 2,$$

and the symbol $[A]$ denotes the integral part of a rational number $A$.

From the above property of the values $D_{\mu m}(\mu = 1, 2)$ it is obvious that in the right-hand side of (9) only items with index $l = l_1 N_\mu$ $(\mu = 1, 2;\ l_1 = 0, \pm 1, \ldots)$ are kept and, hence, (8) is a particular case of the expansions (2).

A significant advantage of the representation (8) is that, as follows from (10), the functions $U_{1kn}$ for a fixed value of $n$ are determined completely by the values $U_{2kn_1}$, where $n_1 \leq n - 1$. Thus, the boundary values of function $V(z, t)$ can be calculated by approximations in powers of the parameter

$$\Delta_0 = \exp(-2\pi\Delta/H) < 1.$$

The inversion of the operator on the left-hand side of (9) allows to express each value $U_{\mu kn}$ $(\mu = 1, 2)$ as a recurrence formula.

It can be seen from the obtained results that, for a potential interaction of cascades $(J = J_1 = J_2 \equiv 0)$, the dependence of the velocity disturbance on the gap $\Delta$ between them can be expressed explicitly. This circumstance is useful for the analysis of the hydrodynamic effects arising for small gaps, when potential interaction is dominant.

Introduction of the function $J(z)$ is needed because the cascade located downstream interacts with the vortical wakes that arise behind the airfoils of the previous cascade owing to trailing vortices in the flow (Figure 2a). To calculate $J$, the theory of a self-similar turbulent vortical wake, which is determined completely by the empirical factor of profile losses $\zeta^*$, is used here. In the theory of hydrodynamic cascades the function $J(z)$ can be set as (see [19, 20]):

$$V_1 + J(z) = V_1 \begin{cases} 1, & \text{out of vortical wakes} \\ 1 - \dfrac{\zeta^* \cdot h_1 \cdot \cos\alpha}{h(\xi_m)} \cos^2(\pi \cdot \eta_m / h(\xi_m)), & \text{in the zone of vortical wake} \end{cases} \tag{11}$$

$$h(\xi_m) = 1{\cdot}52\sqrt{\zeta^* \cdot h_1 \cos\alpha}\sqrt{\xi_m + b}; \quad m = 0, \pm 1, \ldots; \quad \xi_m + \mathrm{i}\eta_m = (z - z_m) \cdot \mathrm{e}^{\mathrm{i}\alpha}.$$

Here $z_m$ is the complex coordinate of the trailing edge of the $m$th airfoil of a cascade 1; $V_1 = |V_1|\mathrm{e}^{-\mathrm{i}\alpha}$ is the complex conjugate time-averaged velocity in a flow core behind cascade 1; $h = h(\xi_m)$ is the width of the vortical wake. The parameter $b$ is determined from the condition $h(0) = 1{\cdot}21d$, which is equivalent to the condition of finite thickness of a vortical wake in the trailing edge whose diameter is equal to $d$. The constants in equality (11) and the form of the function $J(z)$ are determined as a result of systematic wind-tunnel tests of a large number of airfoil cascades [19, 20].

When flow escapes from trailing edges continually, the interaction of cascades results in a change of flow velocity circulation $\Gamma$ on the airfoils. From here, according to the theorem of total vorticity preservation in a continuous flow, vortices appear, which are translated by the stream. They are located in the region of the vortical wakes. In the classical theory of flow around airfoils with small periodic disturbances, the layer of free vortices is usually simulated by a line of contact discontinuity of a tangent velocity located along the critical line of the basic stationary flow. The condition of the absence of a static pressure jump across the contact discontinuity line results in a formula for the local velocity discontinuity

$$\gamma(\tau, t) = -\frac{1}{V_0(\tau)} \frac{\partial \Gamma}{\partial t}\bigg|_{t=t_1}, \quad t = t_1 + T(\tau), \quad T(\tau) = \int_0^\tau \frac{\mathrm{d}\tau}{V_0(\tau)}, \tag{12}$$

where $V_0(\tau)$ is a stationary flow velocity at the point with the arc coordinate $\tau$ counted from the trailing edge along the critical line of the flow.

The complex conjugate velocity induced by the line of the contact discontinuity $L_\mu$ behind the $\mu$th $(\mu = 1, 2)$ cascade equals

$$J_\mu(z, t) = \frac{1}{H\mathrm{i}} \int_0^\infty \sum_{m=0}^{N_\mu - 1} \gamma_{\mu m}(\tau, t) \frac{\mathrm{d}\tau}{1 - \exp[2\pi(\zeta_\mu(\tau) - z + \mathrm{i}mh_\mu)/H]}. \tag{13}$$

Here $\zeta_1 \in L_1, \zeta_2 \in L_2$; $\gamma_{\mu m}$ is determined from (12); $\tau$ is the arc coordinate of line $L_\mu$.

In connection with the use of formulas (12) and (13), it is necessary to notice that integral (13) diverges in case of a smooth trailing edge, where $V_0(\tau) \sim \tau$ near $\tau = 0$. Therefore, in calculations it is necessary to assume the trailing edge to be angular with an internal corner $< \pi$.

The model of the contact discontinuity line, which is widely used in unsteady aerodynamics, describes well the influence of free vortices on the aerodynamic loadings acting on an airfoil. However, for the description of the interaction of unsteady (periodic) vortical wakes with a downstream cascade, and also to estimate the gas-dynamic losses caused by dissipation of the free vortices, the applicability of the model raises some doubts. In this connection, the solution of the problem regarding the diffusion of a contact-discontinuity line in a uniform viscous flow (Figure 2b) is used here to describe the interaction of free vortices behind cascade 1 with cascade 2. In this case the function $J_1(z,t)$ behind the $m$th airfoil of cascade 1 is determined by (see [4])

$$J_1(z,t)=\frac{V_1}{\sqrt{\pi}}\left[\Phi\left(\sqrt{\frac{Re}{4h_1\xi_m}}\,\eta_m\right)-\frac{\sqrt{\pi}}{2}\operatorname{sgn}(\eta_m)\right]\cdot\left.\frac{\partial\Gamma_{1m}}{\partial t}\right|_{t=t_1},\quad t_1=t-\xi_m/V_1,\ z=\xi_m+\eta_m, \tag{14}$$

where $\Phi(\theta)=\int_0^\theta \mathrm{e}^{-\theta^2}\mathrm{d}\theta$ is the error function, $\mathrm{Re}=V_1h_1/\nu_0$ is the Reynolds number, $\nu_0$ is the kinematic viscosity. Thus, the vortical wake of cascade 1 contains near its axis a diffusion layer of periodic free vortices. As follows from the properties of the integral $\Phi(\theta)$, according to (14) the diffusion-layer width is of the order of $1/\sqrt{\mathrm{Re}}$, which is rather small in comparison with the width of a stationary vortical wake for Reynolds numbers $\sim 10^5$–$10^6$, which are typical for gas-turbine engines. The question regarding the real structure of a free-vortices diffusion layer will be considered in Section 5.

The condition of an attached flow on the cascade airfoils at each moment of time leads to the equalities

$$\begin{aligned}
&\Im\mathfrak{m}_i[V_{\mu\,\mathrm{rel}}(z_\mu,t)\,\mathrm{e}^{i\alpha_\mu}]=0,\quad \mu=1,2,\\
&V_{1\,\mathrm{rel}}(z_1,t)=V_1(z_0,t)+J_1(z_0,t),\quad z_0\in L_{10},\\
&V_{2\mathrm{rel}}(z_2,t)=V_2(z,t)+J_2(z,t)+iu+J(z,t)+J_1(z,t),\quad z\in L_{20},
\end{aligned} \tag{15}$$

where $\alpha_\mu$ is the angle between the tangent at point $z$ and the $Ox$-axis for a positive (anticlockwise) motion along the contour $L_{\mu0}$; $V_{\mu\mathrm{rel}}$ is the relative complex conjugate flow velocity on an airfoil of the $\mu$-th cascade.

The functions $J_1(z_0,t)$ and $J_2(z,t)$ in (15) are determined by the equalities (13) and according to (12) depend linearly on the circulation of the relative flow velocity on airfoils of cascades 1 and 2. The values $J$ and $J_1$ in the expression for $V_{2\mathrm{rel}}$ are specified by the equalities (11) and (14) and, therefore, are determined by a profile loss factor $\zeta^*$ for cascade 1 and by circulation of the relative flow velocity on its airfoils. Assuming $z_0=z+iu(z\in L_{20})$, it is easy to formally represent the functions $J=J(z,t)$ and $J_1=J_1(z,t)$ in the form of an expansion such as (8) whose coefficients are expressed by a quadrature and depend on the gap $\Delta$ between the cascades [4].

Substitution of (15) in (9) results in an integral equation with respect to the real (on i) functions

$$U_\mu(s)=\Re\mathfrak{e}[V_{\mu\,\mathrm{rel}}(z_\mu,t)\,\mathrm{e}^{i\alpha_\mu(s)}],\quad z_1=z_0\in L_{10},\ z_2=z\in L_{20},$$

where $s$ is the arc coordinate of a point, counted from the trailing edge of airfoil $L_{10}$ or $L_{20}$ in a positive direction around the contour.

The required function $U_\mu(s,t)$ may obviously be presented as an expansion of the kind (8). An essential difference between such an expansion and the case of potential interaction of cascades consists in the fact that its coefficients depend on the gap between cascades, $\Delta$. It

is easy to show that, for a fixed value of $\Delta$, the convergence of series (8) for $U_\mu(s,t)$ is guaranteed. However, a practically necessary number of approximations in powers of the parameter $\Delta_0$ must be determined during the calculations. Clearly, the number of approximations depends on the behavior of the vortical wake as determined by Equation (11).

Finally, the system of integral equations for the coefficients $U_{\mu kn}(s)$ in expansion (8) of the functions $U_\mu(s,t)$ is given by

$$K_{1k}[U_{1kn}] = \Pi_{1kn}[U_{2pq}], \quad |p| \le q \le n-1,$$
$$K_{2k}[U_{2kn}] = \Pi_{2kn}[U_{1pq}], \quad |p| \le q \le n,$$
$$K_{\mu k}[U_{\mu kn}] = \frac{1}{2}U_{\mu kn} - \frac{e^{i\alpha_\mu(s)}}{Hi}\oint_{L_{\mu 0}} U_{\mu kn}(\sigma)\cdot\sum_{m=0}^{N_\mu-1} e^{j2\pi km\psi_\mu}\left\{\frac{1}{1-\exp[2\pi(\zeta(\sigma)+imh_\mu - z_\mu)/H]}\right.$$
$$\left. - \int_0^\infty \frac{j2\pi k\omega t}{V_{1\mu}(\tau)}\frac{\exp[-j2\pi k\omega T(\tau)]d\tau}{1-\exp[2\pi(\zeta_\mu(\tau)+imh_\mu - z)_\mu/H]}\right\} d\sigma. \tag{16}$$

Here $z_\mu = z_\mu(s) \in L_{\mu 0}$, $\zeta_\mu \in L_\mu$, and $V_{1\mu}$ $(\mu = 1,2)$ is the velocity of spreading of free vortices behind the $\mu$th cascade. The right-hand side $\Pi_{1kn}$ of the first equation in (16) is easy to determine from Equation (10). In order to determine $\Pi_{2kn}$ from the expression for $\Pi_2$ in (10), it is necessary to take into account the representations of the functions $J = J(z,t)$ and $J_1 = J_1(z,t)$ as the series (8).

For fixed values of $n$ the integral equations (16), as well as in the case of potential interaction of cascades, are solved sequentially on the initial airfoil $L_{\mu 0}$ $(\mu = 1,2)$ of one of the cascades. The uniqueness of the solution is ensured by the Kutta-Joukowski condition which demands that the velocity on a sharp trailing edge of airfoils remains finite. The real (in i) parts of (16) are Fredholm integral equations of the second kind. For closed piecewise smooth airfoils $L_{\mu 0}(\mu = 1,2)$ they are solved numerically by approximating an airfoil by an inscribed polygon, on which parts the required function is assumed to be constant [21]. For replacement of such an airfoil by the cumber line, the imaginary part of the equation of the form (16) is used. The solution of this equation allows to obtain the difference of the relative flow velocity on the pressure and the suction surfaces. The kernel of the integral equation is singular in this case and the method of singularities is used to obtain the numerical solution.

As can be seen from the construction of Equations (16), it is assumed that the flow around cascade 1 is unsteady as a result of the potential effect of cascade 2 which, besides potential disturbances, experiences the influence of periodic vortical wakes of cascade 1. An essential aspect of the theory is related to the fact that the inverse effect of flow disturbances produced by cascade 2 on vortical wakes is not taken into account in the determination of the effect of vortical wakes on cascade 2. It should be noted that the effects of vertical-wake evolution in a non-uniform flow [22] have shown to be of little influence on the level of variable loadings for typical turbomachine cascades.

### 3.2. Comparison with experiment and some features of hydrodynamic interaction of cascades

Figure 3 shows the results obtained in [23] of the measured quantity

$$\lambda_2(\Delta) = \frac{\max\limits_{(0,T_2)} Y_2(t) - \min\limits_{(0,T_2)} Y_2(t)}{Y_{20}},$$

where $Y_2$ is the aerodynamic loading, acting along the front of an airfoil belonging to cascade 2, and $Y_{20}$ is its time-averaged value. The measurements were carried out over the mean

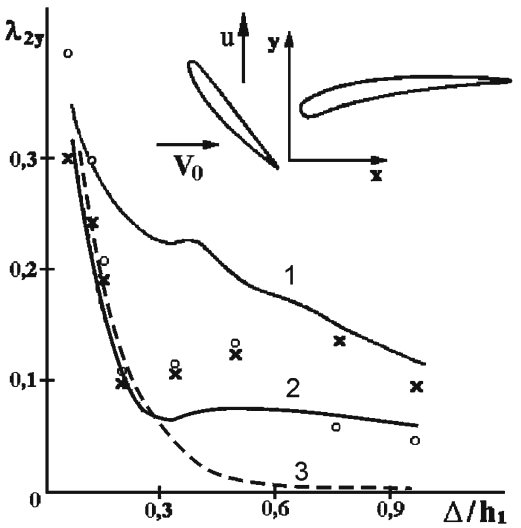


*Figure 3.* Level of exciting forces as a function of axial gap. 1 – calculation by the model of potential-vortical flow, 2 – calculation by the model of potential-vortical flow in quasi-steady statement ($J \neq 0,$), $J_1 = J_2 = 0$), 3 – calculation by the model of only potential flow, o, x – the experimental data at $N_1 = 9$, $N_2 = 10$, $\tau_1 = 0{\cdot}71$, $\tau_2 = 1{\cdot}33$.

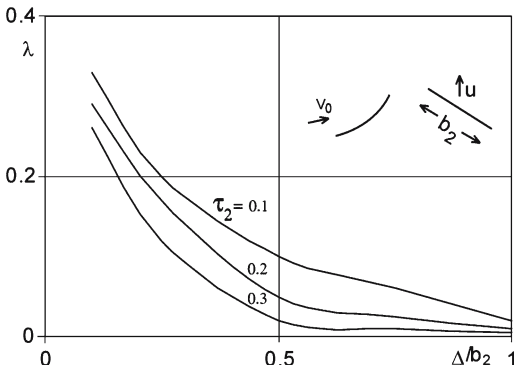


*Figure 4.* Additional circulation as a function of gap between cascades.

radius of the stator for a stage in a low-speed (Mach Number $\sim 0{\cdot}06$) axial compressor. The geometrical parameters of the cascades are given in Figure 3.

The value $\lambda_{2y} = \lambda_{2y}(\Delta)$ obtained by a numerical solution of Equations (16), and the subsequent calculation of the pressure by the Cauchy-Lagrange formula, are presented in Figure 3 for these cases: potential interaction of cascades ($J = J_1 = J_2 \equiv 0$, curves 3); the quasi-stationary solution ($J \neq 0$, $J_1 = J_2 \equiv 0$, curves 2), and full calculation (curves 1). In these calculations the coefficient of the profile losses $\zeta^*$ was set at $0{\cdot}021$.

As can be seen from a comparison of experimental and theoretical results, in the region of small gaps $\Delta$ between cascades, the effects of potential interaction of the cascades dominate. For $\Delta \ll 1$ the properties of the hydrodynamical of the cascades follow from a decomposition (8). For $\Delta \to 0$ the amplitudes of the time harmonics increase because $\Delta_0$ is close to unity. In particular, the time-averaged (a "zero" harmonic) velocity on the airfoil of the $\mu$-th cascade is equal to

$$V_\mu(z_\mu) = U_{\mu 00} + \sum_{n=1}^{\infty} U_{\mu 0n} \cdot \mathrm{e}^{-2\pi n \Delta / H}, \quad \mu = 1, 2,$$

where $U_{\mu 00}(\mu = 1, 2)$ is determined by the relative flow velocity at the inlet of the $\mu$-th cascade for $\Delta = \infty$.

As an example, we show in Figure 4 the dependence of the quantity

$$\lambda_2(\Delta) = \frac{\Gamma_{20}(\Delta) - \Gamma_{200}}{\Gamma_{200}}$$

on $\Delta$, where $\Gamma_{20}$ is the time-averaged velocity circulation on an airfoil of cascade 2, and $\Gamma_{200}$ is its value corresponding to $\Delta = \infty$. The function $\lambda = \lambda(\Delta)$ is calculated by the solution of Equations (16) in the case when cascade 1 is a dense cascade of arcs, and cascade 2 is a widely spaced cascade of plates. In the above cases the integral equation (16) are solved analytically [1] and the values $V_\mu(\mu = 1, 2)$ are approximately equal to

$$V_1 = u_{100} + \sum_{k=1}^{2} [u_{1kk}\cos(2\pi k\omega t) + v_{1kk}\sin(2\pi k\omega t)] \cdot e^{-2\pi k\,\Delta/h_2}$$

$$V_{20} = u_{200} + u_{220} e^{-4\pi k\,\Delta/h_2}.$$

The solidity of cascade 2 is denoted in Figure 4 by $\tau_2 = b_2/h_2$ ($b_2$ is the chord length).

As can be seen from the obtained data, the effect of an axial gap on the time-averaged fluid deflection in a cascade may be significant. It is related to the backward effect on the given cascade of velocity pulsations exerted by it on the next cascade.

Relatively large values of the amplitudes of the harmonics, with $m = 1, 2, \ldots$, which for cascade 2 correspond to the conditions $m \cdot h_2/h_1 = 1, 2, \ldots$, and for cascade 1 to conditions $m \cdot h_1/h_2 = 1, 2, \ldots$, is also a characteristic property of cascade interaction for small gaps $\Delta$. According to expansion (2), the specified values of $m$ correspond to those harmonics of the velocity disturbances that act in phase on the airfoils of cascade 1 or 2. It should be noted that an increased aerodynamic reaction for flow disturbances that are in-phase with respect to airfoils of the cascade, is related to an additional time-averaged flow turn and is not restricted to small gaps $\Delta$.

The significant effect of the parameter $N_1/N_2 = h_2/h_1$ on the level of unsteady loading acting on mutually moving cascades is a result of the above property. Results of a calculation of $\lambda_{2y}$ for potential interaction of two cascades of curvilinear arcs are presented in Figure 5. The calculations were carried out within the range $\frac{6}{7} \leq N_1/N_2 \leq \frac{16}{7}$ for constant dimensionless gap $\Delta/h_1$ and cascade solidities $\tau_1$ and $\tau_2$. Around the values $N_1/N_2 = 1/2, 1, 2$, local maxima of $\lambda_{2y}$ are observed. The significant gradients around the point $N_1/N_2 = 1$ point to possible numerical errors caused by the replacement of the valid relation $N_1/N_2$ by a relation close to it with lower values of $N_1$ and $N_2$. Using an exact representation of $N_1/N_2$ in the analysis of unsteady aerodynamic loadings is important for determining the level of the harmonics exciting the resonant vibrations of blades in a turbomachine stage. Some experimental data confirming the character of dependence of unsteady loadings on $N_1/N_2$ are presented in [20]. Results of numerical modeling are presented in [12].

In the region of moderate gaps, $0{\cdot}15h_1 \leq \Delta \leq 0{\cdot}5h_1$, which are typical for the majority of turbomachines, potential and vortical interactions of cascades can be comparable. As can be seen in Figure 3, in the specified region of the $\Delta$-variation the difference between the theoretical and experimental data is most pronounced. Undoubtedly this is due to the

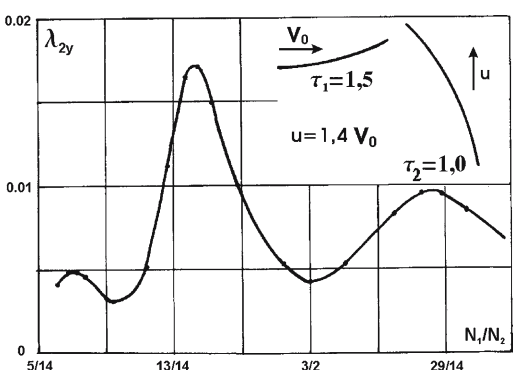


*Figure 5.* The level of exciting forces on the second cascade as a function of the ratio of numbers of airfoils.

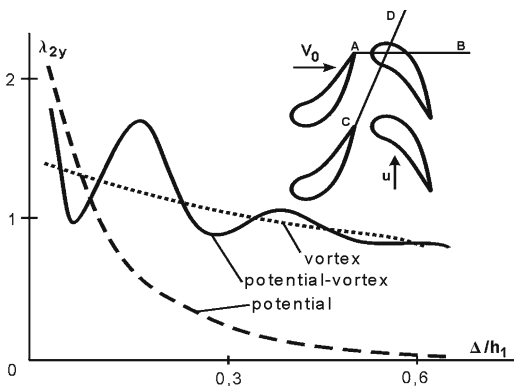


*Figure 6.* Non-monotonic dependence of a level of exciting forces on the axial gap between cascades.

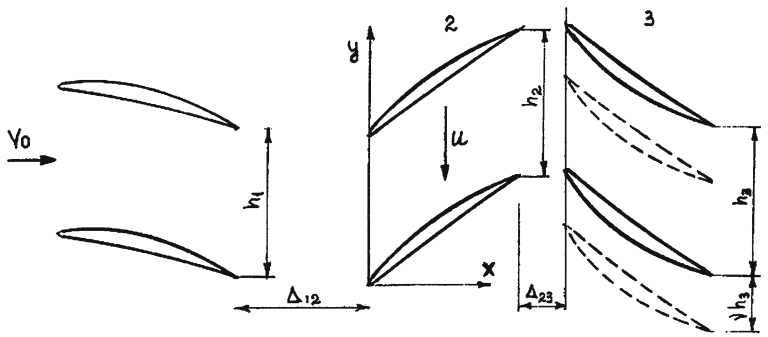


*Figure 7.* Stator-rotor-stator cascades of airfoils.

adequacy of the used model of periodic vortical wakes of cascade 1. It is interesting to note that, for the presented examples, a quasi-stationary solution ($J_1 = J_2 \equiv 0$) is more satisfactory when the potential interaction is precisely taken into account, and a widely accepted theory of self-similar vortical wakes behind the upstream cascade is used.

One feature of cascade interaction in the region of moderate gaps is clearly visible in Figure 3 and has also been noted in experiments [24]: a non-monotonic dependence of $\Delta$ of the level of unsteady loading on cascade 2. This result seems paradoxical, since it does not correspond to the widespread idea that an increase in the axial gap between blade rows inevitably results in a reduction of the pressure pulsations caused by rotor-stator interaction. The calculation performed under the stated theory for turbine cascades is presented in Figure 6. Here the dependencies $\lambda_{2y} = \lambda_{2y}(\Delta)$ are related to the potential, vortical, and potential-vortex interactions of cascades. The first two curves show a monotonous decrease of $\lambda_{2y}$ with increasing $\Delta$. A full calculation of potential-vortex interaction, however, results in a significant non-monotonicity of the dependency $\lambda_{2y} = \lambda_{2y}(\Delta)$. The most evident explanation of this phenomenon is that potential disturbances behind cascade 1 propagate perpendicularly to the front of the cascades (along line AB), whereas the wake (convective) flow disturbances propagate mainly along the streamlines of the relative flow. For different gaps $\Delta$ this circumstance results in different phase displacements between the specified disturbances on an airfoil of cascade 2 and, as a result, in different total disturbances on them. Clearly, for a sufficient widening of the axial gap, vortical and potential-vortex disturbances come closer and the rotor-stator interaction can be described by the effect of only vortical wakes behind cascade 1 on cascade 2.

## 4. Flow in a cascade moving between two motionless cascades

In multistage turbomachines each blade row, except for the extreme ones, interacts with the two next stators or rotors. In the 2D problem statement this corresponds to a flow around three cascades of the type stator-rotor-stator or rotor-stator-rotor. If one assumes the flow upstream of the cascades to be uniform, the middle cascade is subjected to the joint effects of the disturbances caused by the cascades located upstream and downstream. In this section, we investigate some features of periodic flows through the specified set of three cascades.

### 4.1. Effect of the mutual position of extreme cascades

Figure 7 shows a set of cascades of the stator-rotor-stator type, where it is assumed for definiteness that the middle cascade 2 moves at a speed "$u$" in the negative direction of the $Oy$-axis with respect to cascades 1 and 3. When the interaction of extreme cascades is

neglected, then, in accordance with expansion (2), the velocity disturbance of the incompressible flow on an airfoil of cascade 2 may be written as

$$V_2(x, y, t) = \sum_k [V_k^{(12)}(x, y, \Delta_{12}) e^{j2\pi k y/h_1} \cdot e^{-j2\pi k ut/h_1} + \\ + V_k^{(23)}(x, y, \Delta_{23}) e^{j2\pi k y/h_3} \cdot e^{-j2\pi k ut/h_3}], \tag{17}$$

where $h_\mu (\mu = 1, 3)$ is the pitch of the $\mu$-th cascade; the point $(x, y)$ belongs to an airfoil of cascade 2; $\Delta_{12}$ and $\Delta_{23}$ are the gaps between cascades 1-2 and 2-3, and the superscripts (12) and (23) of the coefficients $V_k$ correspond to interactions of pairs of the cascades 1-2 and 2-3, respectively.

In (17) $t = 0$ is assumed to correspond to a certain mutual circumferential position of the airfoils of cascades 1 and 3. The ordinate $y_0$ in the stator reference frame is related to $y$ by the relation $y = y_0 + ut$. Thus, if one assumes that, for example, cascade 3 is shifted with respect to cascade 1 along the front over a distance $\Delta y_0 = \nu \cdot h_3$ in the direction of motion of cascade 2, it corresponds to a shift of the time phase of interaction of the cascades 2 and 3 equal to $\Delta t = \nu h_3/u$.

Further let the pitch of one of the cascades 1 or 3 contain integer $\chi = 1, 2, 3\ldots$ pitches of the other of the specified cascades, *i.e.*, for example, $h_1 = \chi h_3$. Then (17) becomes

$$V_2(x, y, t) = \sum_k [V_{\chi k}^{(12)} + e^{-j2\pi k\nu} V_k^{(23)} + \\ + \sum_{m=1}^{\chi-1} V_{\chi k+m}^{(23)} \cdot e^{j2\pi m y/h_1} \cdot e^{-j2\pi m ut/h_1}] \cdot e^{j2\pi k y/h_3} \cdot e^{-j2\pi k ut/h_3}. \tag{18}$$

From (18) follows, that amplitudes of harmonic fluctuations with frequencies such as $ku/h_3$, where $k = 1, 2, 3\ldots$, depend on $\nu$, *i.e.*, from mutual displacement of the cascades 1 and 3. The specified property is similar to an interference of two synchronous sources of disturbances. If the pitches of the cascades 1 and 3 are identical, *i.e.*, $h_1 = h_3$ $(\chi = 1)$, then all harmonics of velocity disturbances $V_2$ from both cascades will interfere. If the common period of cascades 1 and 3 is equal, namely $H_s = N_1 h_1 = N_3 h_3$, where $N_1$ and $N_3$ are mutually prime numbers, then harmonics of disturbances with frequencies of such as $kN_1N_3u/H_s$, where $k = 1, 2, 3, \ldots$, interfere.

As an illustration of the effectiveness of the mutual shift of the cascades 1 and 3, the dependencies on $\nu$ of the relative jump $\Delta\Gamma_2$ of the flow velocity circulation $\Gamma_2(t)$ on the period $T = u/H_s$ on an airfoil of cascade 2 are presented in Figure 8, that is,

$$\Delta\Gamma_2(\nu) = \Gamma_{200}^{-1} \left[ \max_t \Gamma_2(t) - \min_t \Gamma_2(t) \right], \quad t \in (0, T),$$

where $\Gamma_{200}$ is the time-averaged value of $\Gamma_2$, which does not depend on $\nu$ according to (18). The determination of the values of $V_k^{(12)}$ and $V_k^{(23)}$ $(k = 0, \pm 1, \ldots)$ was carried out by means of the theory of potential-vortical interaction of cascades in the quasi-stationary problem formulation. The cascade geometry is shown in Figure 7 for gaps between the cascades equal to $\Delta_{12} = 0{\cdot}84h_1$ and $\Delta_{23} = 0{\cdot}27h_3$. The coefficients of the profile losses of the cascades 1 and 2 were taken equal to $\zeta^* = 0{\cdot}023$, and the relation $h_3/h_1$ was varied: $h_3/h_1 = 1$ (curve 1); 1/2 (curve 2), and 33/34 (curve 3).

The pulsation level of the velocity circulation on cascade 2 can be seen to depend significantly on the shift of cascade 3 with respect to cascade 1. This effect is most significant for the pitch relation $h_3/h_1 = 1$ and is practically absent for $h_3/h_1 = 33/34$, *i.e.*, when $N_1$ and $N_3$

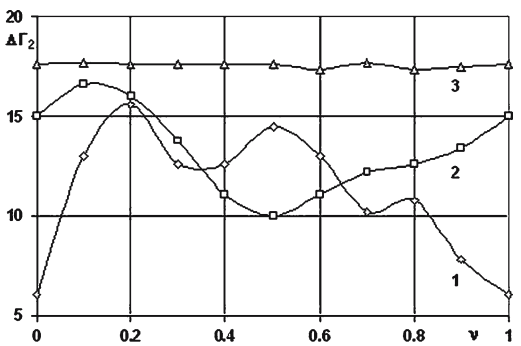


*Figure 8.* Relative variation of computed velocity circulation $\Delta\Gamma_2$ on cascade 2 as a function of mutual position $\nu$ of cascades 1 and 3. $1 - h_3/h_1 = 1$; $2 - h_3/h_1 = 1/2$; $3 - h_3/h_1 = 33/34$.

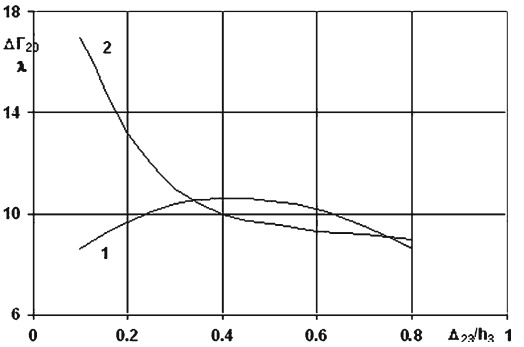


*Figure 9.* Averaged level of computed unsteady circulation $\Delta\Gamma_{20}$ on an airfoil of cascade 2 (curve 2) and effect of mutual shift of cascades 1 and 3 ($\lambda$, curve 1) as a function of relative gap $\Delta_{23}/h_3$ between cascades 2 and 3.

are mutually prime numbers. It is typical that in the latter case the average pulsation level is maximal.

It follows from the obtained results that the pulsation level of the flow velocity circulation on a cascade interacting with two cascades located upstream and downstream is characterized not only by its averaged value

$$\Delta\Gamma_{20} = \int_0^1 \Delta\Gamma_2(\nu)\ \mathrm{d}\nu,$$

but also by the value of the variation of $\Delta\Gamma_2(\nu)$ in the interval $0 < \nu < 1$,

$$\lambda = \max_{\nu} \Delta\Gamma_2(\nu) - \min_{\nu} \Delta\Gamma_2(\nu).$$

According to (18) the values $\Delta\Gamma_{20}$ and $\lambda$ depend on the axial gaps $\Delta_{12}$ and $\Delta_{23}$ that determine the level of interaction of cascade 2 with cascades 1 and 3.

The dependencies $\lambda = \lambda(\Delta_{23})$ (curve 1) and $\Delta\Gamma_{20} = \Delta\Gamma_{20}(\Delta_{23})$ (curve 2) that are presented in Figure 9 were obtained for a fixed axial gap $\Delta_{12} = 0{\cdot}84h_1$ and the relation $h_3/h_1 = 1$. The monotonic decrease of $\Delta\Gamma_{20}$ with increasing $\Delta_{23}$ is obviously related to the asymptotic decrease of the upstream effect of cascade 3. At the same time, the value $\lambda = \lambda(\Delta_{23})$ describing the effect of a mutual shift of cascades 1 and 3, reaches its maximum for that value of $\Delta_{23}$, for which the upstream effect of cascade 3 is comparable to the downstream effect of cascade 1. It should be noted that, contrary to a widespread belief, this situation is typical for turbomachine operations with axial gaps between blade rows that are quite common.

It is now clear that the effect of mutual displacement (clocking) of stators in a cascade system of stator-rotor-stator type can be described by the theory of potential-vortical interaction of cascades. Practically, the specified effect affords an opportunity of reducting periodic flow-velocity pulsations, caused by rotor-stator interaction. This reduction can be achieved by optimization of the axial gaps between rows, the number of blades in them and a mutual circumferential arrangement of bordering rows.

Within the framework of the considered model of cascade interaction at clocking of the extreme rows, the time-averaged linear aerodynamic loading on the rows does not change. However, according to Section 3, significant variation of circulation on cascade 2 results in a corresponding alteration of the intensity of the periodic free vortices that are shed from its

airfoils and result in gas-dynamic losses because of dissipation. It is, therefore, to be expected that the clocking of stators or rotors affects the above losses and, respectively, the total pressure variation in a turbomachine. For the analysis of vortex-formation processes that are caused by the interaction of three cascades of airfoils and to assess the validity of the semi-analytic theory, a numerical simulation of the flow will be carried out.

### 4.2. Numerical method

A numerical method of solution for the unsteady Reynolds-averaged Navier-Stokes equations [25], closed by the two-equation ($q$-$\omega$) turbulence model proposed in [26], is applied here to calculate the turbulent flow of a viscous gas through a cascade system of the stator-rotor-stator type. For each cascade in its own frame of reference a multi-block computational O-H grid is generated with the period along the front equal to the pitch of the cascade, and fixed distances from the inlet and outlet fronts. Thus, for a given moment of time, the computational flow domain through the set of three cascades forms a compound grid, with the common period along the front equal to $H = N_1 h_1 = N_2 h_2 = N_3 h_3$. The fragment of such a grid for the cascades shown in Figure 7 for $N_1 = N_3 = 34$, $N_2 = 35$ is presented in Figure 10. Here the O-type grid, which is generated in the vicinity of each airfoil, contains $100 \times 16$ grid points, and the H-type grid contains $81 \times 33$ grid points on one pitch of each cascade. The total number of grid points was 440119.

On the airfoil surface boundary the no-slip and adiabatic wall ($\partial T/\partial n = 0$) conditions are imposed on the turbulence variables: $q = \partial\omega/\partial n = 0$.

On the left (inlet) domain boundary the stagnation temperature, total pressure, and the flow angle, and on the right (outlet) boundary the static pressure, were specified. The turbulence parameters $q_\infty, \omega_\infty$ were fixed on the inlet boundary. On the zonal boundaries of the adjacent cascade grids, flux conservation is maintained. This is similar to the approach proposed in [27].

The required solution has period $H$ along the front of the cascades. This period can contain a various, including $\neq 1$, number of pitches of each of the cascades (a condition of the generalized periodicity). In the numerical scheme the performance of the specified condition is provided by the requirement of coincidence during each moment of time of the solution in points that are separated a distance $H$ from one another along lines parallel to the front of the cascades.

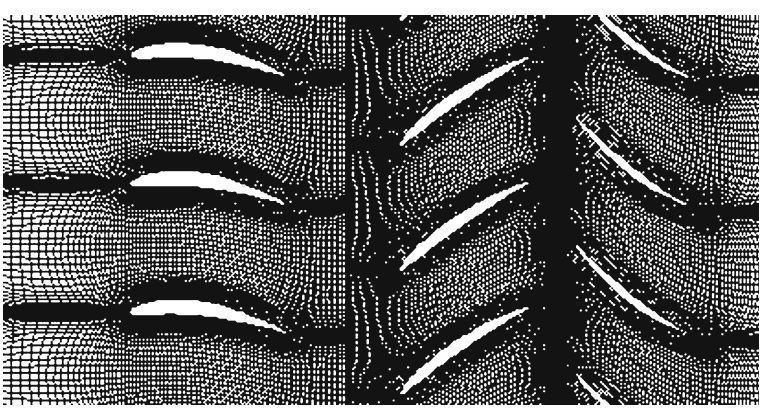

*Figure 10.* Fragment of a computational grid for 3 cascades stator-rotor-stator ($N_1 = N_3 = 34$, $N_2 = 35$).

We have used a numerical method to solve the Navier-Stokes equations that is based on Godunov's scheme with increased high order of accuracy [25]. The method allows us to obtain numerically a steady solution of second-order accuracy in the spatial variables and first-order accuracy in time. The system of equations for the turbulence parameters $q$ and $\omega$ is written in divergence form and is solved similarly.

With flow parameters prescribed at the inlet and outlet boundaries of the computational domain and a given speed $u$ of cascade 2, the calculations were carried out until a periodic solution was obtained.

Figure 11 shows a portion of the instant entropy contours obtained for the grid presented in Figure 10. The data were obtained for atmospheric conditions for an axial inlet flow ($\alpha = 0$) and $u = 262{\cdot}5$ m/s. On the presented portion the evolution of vortical wakes behind cascades 1 and 2 is quite visible, and the phase displacement on the next airfoils of cascade 2 is clearly observed.

It should be noted that the computing time required for obtaining the periodic solution is essentially longer than the time required for obtaining the stationary solution, and it certainly depends strongly on the number of computational grid points. For real blade numbers, even the 2D unsteady numerical simulation is extremely laborious. On the other hand, as was noted in Section 3, an artificial reduction of the numbers $N_\mu$ ($\mu = 1, 2, 3$) can change significantly the parameters of the periodic flow. For large variations of the initial data (including the parameter $\nu$) these circumstances force one to resort to a computing grid with rather a small number of grid points. This, in turn, requires a careful analysis of the numerical results. If it is necessary to substantially increase the number of grid points with a corresponding reduction of the initial data, the numerical solution is considered as an independent (in relation to physical) experiment; see below.

### 4.3. Comparison with experiment and some effects of stators clocking

Experimental research regarding the unsteady interaction of a system stator-rotor-stator rows was carried out on a model of an axial compressor. Static pressure pulsations on the rotor case, total pressure pulsation behind a rotor and behind a stage, and also the unsteady velocity field behind a rotor were measured by a two-component laser anemometer. The

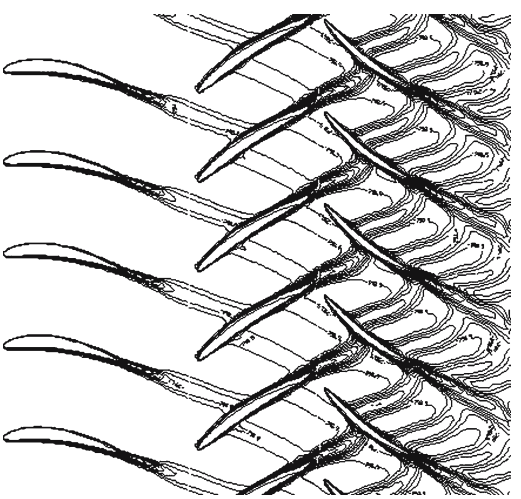

*Figure 11.* Entropy contours for three cascades stator-rotor-stator ($N_1 = N_3 = 34$, $N_2 = 35$).

experiments and the technique for processing the measured data were based on the analysis of flow kinematics in mutually moving rows (see Section 2). The comparisons of theory and experiment presented here refer to various physical effects of a mutual circumferential shift of the stators.

4.3.1. *Flow pulsations on rotor blades*

The system of cascades shown in Figure 7 corresponds to the cylindrical section on the mid-span radius of a subsonic axial compressor designed with the following parameters: total pressure ratio 1·31; adiabatic efficiency 0·88 at a rotor-blade-tip speed 300 m/s; hub/tip ratio diameter 0·75. The number of vanes in the stators (rows 1 and 3) is equal to 34, and number of blades in the rotor (row 2) is equal to 35. The axial gaps on mid-span radius are $\Delta_{12} = 0{\cdot}84h_1$; $\Delta_{23} = 0{\cdot}27h_3$, respectively.

Figure 12 shows experimental and computed values of $\Delta E(\nu) = \sqrt{\int_0^1 \Delta\varepsilon^2 \, \mathrm{d}y_0}$, where

$$\Delta\varepsilon = \frac{\varepsilon(x, y_0) - E(x)}{E(x)} \times 100\%, \quad \varepsilon(x, y_0) = \sqrt{\frac{1}{T_0}\int_0^{T_0} [P(x, y_0, t) - P_0]^2 \mathrm{d}t}, \quad E(x) = \int_0^1 \varepsilon \mathrm{d}y_0.$$

Here the coordinate $y_0$ is related to the general pitch of rows 1 and 3, $h_s = h_1 = h_3$; $T_0 = h_2/u$ is the period of pressure pulsations in the stator frame of reference; $P(x, y_0, t)$ is the instantaneous value of the static pressure on the rotor case, and $P_0$ is its time-averaged value. The value of $P$ was measured by five transducers at regular intervals located along an axis of the compressor from the inlet (transducer no. 1) up to the outlet (transducer no. 5) front of a rotor. Figure 12 shows the results concerning the transducers 1, 3 and 5. The variation of the $y_0$ coordinate is achieved by simultaneous turn of rows 1 and 3, and the variation of parameter $\nu$ is achieved by a turn of row 1 with respect to row 3 in the direction of rotor rotation.

Static pressure pulsations on the casing are caused by its non-uniformity in a rotor blade channel, and according to Section 2, its rms deviation relative to $P_0$ has the circumferential period $h_s$. The value of $\varepsilon$ averaged over the period $h_s$ is denoted by $E$ and corresponds to pulsations $P$ caused by time-averaged aerodynamic loading on the rotor blades. Thus, the quantity $\Delta E$ is a measure of pressure pulsations on the rotor blades caused by their interaction with the next rows.

The calculation of $\Delta E(\nu)$ for a fixed axial coordinate $x$ is executed as a result of the solution of the potential-vortical interaction problem involving three cascades on mid-span radius of a stage. The solution in the rotor blade channel is obtained, upon which the calculation of the coefficients $\Pi_{kl} = P_{kl}$ allows one to proceed in the stator frame of reference $(x, y_0, t)$ in which the measurements are executed.

As can be seen from the obtained data, the stators' clocking affects significantly the rotor-blade pressure pulsations. The theory of potential-vortical interaction describes correctly the character of this effect for subsonic flows and can be used for an estimate of the expected effects related to pressure pulsations caused by rotor-stator interaction.

As was noted above, theoretical values of $P_0$ and $E(x)$ do not depend on $\nu$. In the experiments, the rms deviation on $\nu$ did not exceed 0·13% for $P_0$ and 1·7% for $E$ concerning their mean values.

More complete experimental investigations of the effect of the mutual circumferential stators shift in a system of stator-rotor-stator rows were carried out on a large-sized (external diameter 1·2 m) experimental setup containing in the working part a stage of the axial compressor with inlet guide vanes (IGV) [17]. The stage is designed to have a total pressure ratio 1·05; adiabatic efficiency 0·9, rotor rotation speed 2000 rot/min, mass flow rate 30·8 kg/s, and

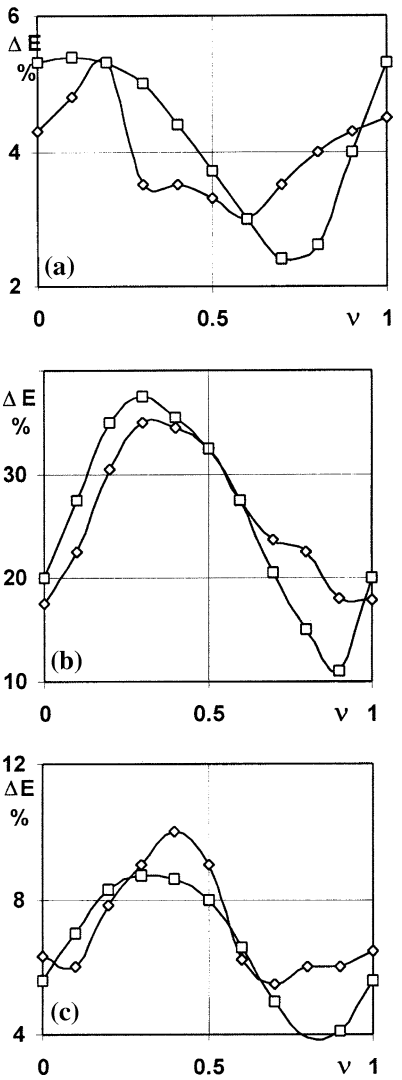


*Figure 12.* Effect of mutual stators shift $\nu$ on RMS value $\Delta E$ of a tangential non-uniformity of static pressure pulsations for transducers No. 1 (a), No. 3 (b), No. 5 (c). ◊ – experiment; □ – calculation.

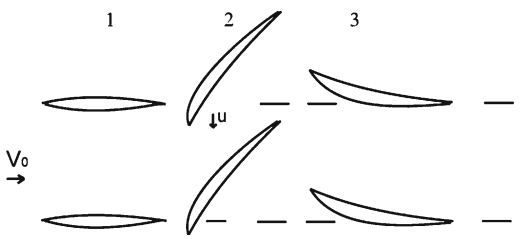


*Figure 13.* Cascades of airfoils in cylindrical section of an experimental stage of the axial compressor.

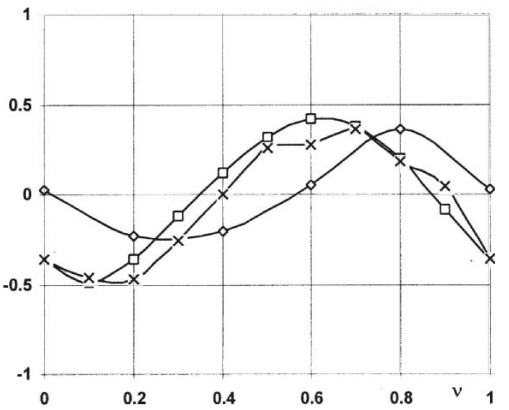


*Figure 14.* Stators clocking effect on radiated noise and comparison with flow pulsations on the rotor blades. □ – calculation, assembly 1, x – experiment, assembly 1, ◊ – experiment, assembly 2.

hub/tip ratio diameter 0·8. The number of vanes in the IGV and stator are equal to 36, and 38 in the rotor. Cascades of airfoils on the cylindrical section of a flowing path on mid-span radius are shown in Figure 13. The theoretical and experimental data presented below are obtained for a design operating mode of the stage.

As follows from (18), for an equal number of IGV and stator vanes, the effect of their mutual circumferential shift depends on the axial gaps $\Delta_{12}$ and $\Delta_{23}$ between the rows. In Table 1, the results of a calculation by the theory of potential-vortical interaction of $\overline{E}$ and $\langle E \rangle$ at various axial gaps, are presented for

$$\overline{E} = \int_0^1 \varepsilon_1(\nu)\mathrm{d}\nu, \quad \langle E \rangle = \sqrt{\int_0^1 \left[\frac{\varepsilon_1(\nu) - \overline{E}}{\overline{E}}\right]^2 \mathrm{d}\nu} \times 100\%,$$

$$\varepsilon_1(\nu) = \sqrt{\frac{1}{T_0}\int_0^{T_0}\left[\frac{\Gamma_2(t)-\overline{\Gamma}_2}{\overline{\Gamma}_2}\right]^2 \mathrm{d}t} \times 100\%,$$

where $\Gamma_2(t)$ is the circulation of the flow on an airfoil of cascade 2 (Figure 13) at $t$, and $\overline{\Gamma}_2$ is its time-averaged value. Here the axial gaps are given for the hub sections and are in mm. The computed results are given as the relation $\overline{E}/\langle E\rangle$.

As can be seen from Table 1, among the considered axial gaps the following sets appear: $\Delta_{12} = \Delta_{23} = 15$ mm and $\Delta_{12} = 60$ mm, $\Delta_{23} = 5$ mm. In both cases the values of the pulsations of the velocity circulation $\overline{E}$ averaged over $\nu$ are close; however, their rms deviations from $\overline{E}$ differ by more than a factor of 2. No doubt, this is due to the fact that, in the second case, the effect on the pulsations of flow velocity on cascade 2 caused by its interaction with cascade 3 is more important than the effect of the vortical wakes of cascade 1.

Measurements of pressure pulsations on rotor blades similar to those presented in Figure 12 and executed during the investigated stage for assemblies 1 ($\Delta_{12} = \Delta_{23} = 15$ mm) and 2 ($\Delta_{12} = 60$ mm, $\Delta_{23} = 5$ mm) confirm the calculated prediction [17].

4.3.2. *Generation of noise*

Pressure pulsations on rotor blades are one of the sources of noise generation radiated by a turbomachine on frequencies that are multiples of the rotor-blade passing frequency. It can be expected that a significant variation of the level of pressure pulsations on the rotor blades, owing to a circumferential shift of the next stators, results in a corresponding change in the generated noise.

In Figure 14 for the compressor assemblies 1 and 2 we present the dependencies

$$\varepsilon_0 = \varepsilon_0(\nu) = \frac{L(\nu)-\overline{L}}{\overline{L}},$$

where $L(\nu)$ is the intensity of sound radiated in 1/3 octave band containing the basic rotor-blade passing frequency, and $\overline{L}$ is the value of $L$ averaged over $\nu$. The sound intensity was measured in the inlet plenum located on an entrance in a working part of the experimental setup and confirmed in the reverberation chamber [28]. The variation of the parameter $\nu$ was carried out here by a turn of the stator relative to IGV towards the rotation of a rotor.

For comparison, we show in Figure 14 the quantity

$$\mu(\nu) = \frac{\varepsilon_1(\nu)-\overline{E}}{\overline{E}}$$

*Table 1.* Ratios of $\Delta_{12}$ and $\Delta_{23}$.

| $\Delta_{23}$, mm \ $\Delta_{12}$, mm | 5 | 15 | 25 | 35 | 60 |
|---|---|---|---|---|---|
| 5 | 6·2/40·5 | 4·2/38 | 4·3/27 | 4·3/20·5 | 4·3/15 |
| 15 | 5·8/34 | 4·2/41 | 3·6/34 | – | – |
| 25 | 5·5/30·5 | 3·8/39 | 3·3/34 | 3·1/27·5 | 3·0/21 |
| 35 | – | 3·5/33 | 2·8/33·5 | – | – |

averaged over 13 cylindrical sections of a flowing path from the hub up to the periphery of assembly 1. In each of the sections, the calculation was carried out according to the theory of potential-vortical interaction of cascades.

From the data obtained it is seen that, according to Table 1, the relative change of the intensity of the radiated noise as a result of variations of the parameter $\nu$ is much higher for assembly 1 than for assembly 2. The total variation of the noise, expressed in decibels and determined by the formula

$$\Delta D = 10 \cdot {}^{10}\log \frac{1 + \max\limits_{\nu} \varepsilon_0}{1 + \min\limits_{\nu} \varepsilon_0} [\mathrm{dB}]$$

is 4·5 dB for assembly 1 and 2·1 dB for assembly 2.

A comparison of values $\varepsilon_0 = \varepsilon_0(\nu)$ and $\mu = \mu(\nu)$ serves to show that the calculation by the described theory allows us to estimate the stators' clocking effect on the radiated noise.

4.3.3. *Total pressure losses and vortical wakes of rotor*

In the references [7–13], which are devoted to experimental investigations of the stators' clocking effects, it is shown that the parameter $\nu$ affects the total pressure losses in a stage of a turbomachine. Measurements were carried out, both by a rake probe of total pressure and by probes equipped with high-frequency transducers, which were shifted over the radius and measured the instantaneous values of the stagnation pressure.

As an illustration, we show in Figure 15a (curve 1) the dependence of the quantity

$$\lambda(\nu) = \frac{\Delta P(\nu) - \Delta \overline{P}}{\Delta \overline{P}} \times 100\%$$

on the parameter $\nu$, where $\Delta P$ is the difference in stagnation pressures averaged over time and on a circle and measured on the mid-span radius behind cascade 3 (90 mm from stator trailing front) and behind cascade 2 (11 mm from rotor trailing front), and $\Delta \overline{P}$ is the value of $\Delta P$ averaged over $\nu$. Measurements have been executed on the above-mentioned experimental installation in assembly 1, which on the mid-span radius corresponds to an axial gap $\Delta_{23} = 20{\cdot}5$ mm. A similar dependence obtained by a numerical solution of the Reynolds equations (see Section 4.2) is presented in Figure 15b. The calculations were carried out for $N_1 = N_3 = 18$, $N_2 = 19$.

Traditionally, $\Delta P$ is related to the total pressure losses in the stator, *i.e.*, in cascade 3 (see Figure 13). A detailed analysis of vortical wakes behind the stator of the high-loading model stage of the compressor [13], as well as periodic stagnation pressure pulsations behind cascade 3 [17], has, however, shown that the losses of the total pressure on the stator vanes actually depend weakly on $\nu$ and cannot explain the obtained values of $\lambda = \lambda(\nu)$. The most probable source of the above losses is the dissipation of the periodic free vortices arising in a stage behind the rotor, *i.e.*, behind cascade 2 (see Figure 13).

Direct comparisons of both experimental and computed values of $\lambda = \lambda(\nu)$ with intensity of free vortices are presented in Figure 15. The relative intensity of free vortices was estimated here by the quantity

$$\mu(\nu) = \frac{w_3(\nu) - \overline{w}_3}{\overline{w}_3},$$

where $w_3(\nu)$ is a measure of velocity pulsations in the vortical wakes of cascade 2, and $\overline{w}_3$ is its value averaged over $\nu$.

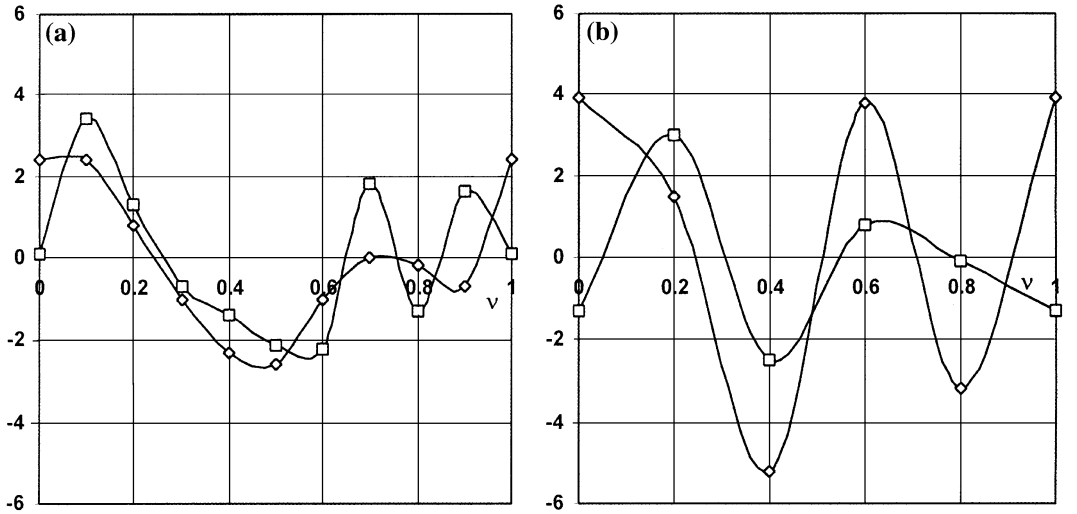


*Figure 15.* Stators clocking effect on total pressure losses $\lambda(\diamond)$ and comparison with the intensity of free vortices $\mu(\square)$. (a) experiment; (b) calculation.

The instantaneous flow velocity $V = V(r, x, y_0, t)$ behind cascade 2 was measured by a two-component laser anemometer, and the measurement point was fixed at a distance of 8·5 mm from the outlet front [18]. As a result of these measurements, the instantaneous projections of the absolute velocity vector on the axial and tangential (along the front) directions in the stator frame of reference, were determined for 129 moments of time at 10 points in regular intervals located on a pitch $h_s$ for 10 values of the parameter $\nu$. On the basis of the obtained data, the expansion coefficients $V_{kl}$ of (2) were calculated for 20 harmonics in time and for 2 harmonics along the $y_0$ coordinate. According to this, the transition to a rotor frame of reference ensured expansion (2); it represents the instantaneous value of the relative flow velocity for 2 harmonics in time and 20 harmonics along the $y$-coordinate. Thus, the time-averaged value of vector $V_0$ of the instant relative velocity $V_{\text{rel}}$ in the rotor frame of reference describes in sufficient detail a stationary vortical wake in the relative flow behind a rotor, and its rms deviation $w_1 = \langle V_{\text{rel}} - V_0 \rangle$ describes the level of velocity pulsations over the tangential period, equal to a pitch of the rotor blades $h_2$ (see Section 2). Further, the value $w_3(\nu)$ was determined by the formula

$$w_3(\nu) = \sqrt{\frac{1}{h_2} \int_0^{h_2} \left[ \frac{w_1(y) - \overline{w}_1}{\overline{w}_1} \right]^2 \mathrm{d}y},$$

where $\overline{w}_1$ is the value of $w_1$ averaged over $h_2$.

As follows from Figure 15, both experimental and computational data show that the ranges of $\nu$ corresponding to increased or lower losses of the total pressure correlate with the variation of intensity of velocity pulsations behind a rotor. It is to be expected that the above velocity pulsations are concentrated in the zones of vortical wakes of airfoils of cascade 2, and the value $\mu$ characterizes the relative change of their intensity at mutual circumferential shift of IGV and stator.

Indeed, the examples of pitch-wise distribution of $w_2 = w_2(y, \nu, t)$, which equals the projection onto the vector $V_0$ of $(V_{\text{rel}} - V_0)/|V_0|$, which is presented in Figure 16, show that velocity pulsations are rather significant in the zone of a stationary vortical wake and are practically

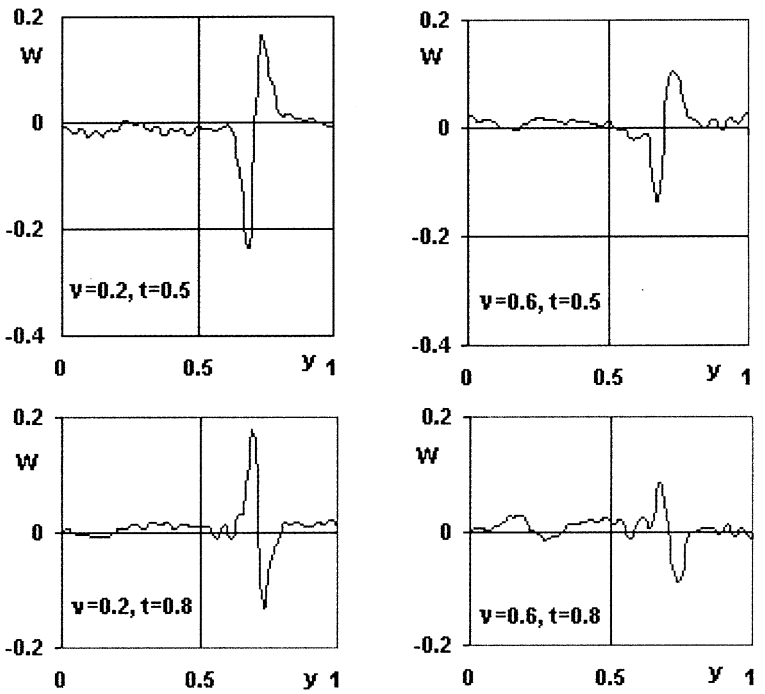


*Figure 16.* Experimental pitch-wise distribution of flow velocity pulsations behind cascade 2.

absent in the stream core. The value of $w_2$ is determined experimentally and presented in Figure 16 for $\nu = 0{\cdot}2$, $0{\cdot}6$ and time: $t/T = 0{\cdot}5, 0{\cdot}8$, when velocity pulsations are in counter-phase.

The data given in Figures 15 and 16 allow us to consider an established fact, namely, that the part of the total pressure losses in the turbomachine stage is caused by flow-velocity pulsations that arise owing to the occurrence of free vortices during rotor-stator interaction.

Comparison of the experimental distributions $V_0 = V_0(y)$ in vortical wakes with numerical results obtained by the self-similar theory is satisfactory for a corresponding choice of the profile-losses coefficient $\zeta^*$ [18]. The numerical solution has been obtained here for a total number of grid points equal to 235015 which allowed 33 grid points on a pitch of cascade 2 and permitted to vary the parameter $\nu$ over a wide-enough range. The value of the velocity $V_0$ averaged over a pitch $h_2$ was close to the experimental one; however, the stationary vertical-wake parameters differed essentially. The experimental and calculated values of $\lambda = \lambda(\nu)$ and $\mu = \mu(\nu)$ are shown in Figure 15. These values agree qualitatively, but in a quantitative sense they differ considerably.

## 5. Periodic vortical wakes of a turbomachine cascade

As follows from the results of Section 4, in a flow around mutually moving cascades of airfoils vortical wakes are formed behind them, which contain periodic flow-velocity pulsations which are especially intensive near the wake axis. From experimental data (see Figure 16) it is easy to conclude that the vorticity of the velocity-pulsation part achieves its maximum (in modulus) values on the wake axis; it is close to zero in the stream core and depends essentially on the unsteady part of the velocity circulation on the airfoil (effect of the parameter $\nu$). Nevertheless, the distribution of the unsteady velocity in a flow behind an airfoil similar

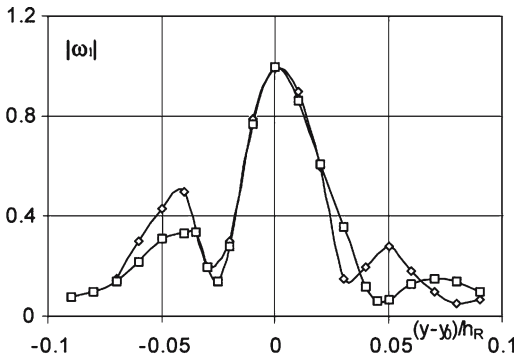


*Figure 17.* Distribution of flow vorticity in a wake of an airfoil of cascade 2. $|\omega_1| = |\Omega_1(y)|/|\Omega_1(y_1)|$. (◇ – experiment, □ – calculation).

to that of Figure 16 differs sufficiently from both the model of contact discontinuity and the model of viscous diffusion assumed in Section 3.

The structure of the vortical wakes containing periodic free vortices has been considered in more detail. Clearly, this problem is related to the definition of energy dissipation in a flow containing free vortices, and goes beyond the scope of the problem of the interaction of hydrodynamic cascades.

### 5.1. Distribution of periodic vorticity in the wake

To investigate the unsteady vorticity behind airfoils of cascade 2 experimentally, velocity measurements similar to those described in Section 4.3.3 have been executed in sections located at distances of 8, 10, and 12 mm from the front outlet. The required vorticity is presented in the form

$$\Omega = \sum_k \sum_l \Omega_{kl}(r, x) \cdot e^{i2\pi l y/h_2} \cdot e^{j2\pi k y/h_s} \cdot e^{-j2\pi k ut/h_s}, \; \Omega_{kl} = \frac{1}{2}\left[\frac{\partial V_{ykl}}{\partial x} - 2\pi\left(i\frac{l}{h_2} + j\frac{k}{h_s}\right) V_{xkl}\right], \tag{19}$$

where $V_{xkl}$, $V_{ykl}$ are the coefficients of expansion (2) for the axial and tangential components of the vector $V - V_0$, respectively, and the derivative $\partial V_{xkl}/\partial x$ was calculated approximately from measurements in three sections.

The numerical solution of the vorticity was carried out under the assumption that $N_1 = N_2 = N_3 = 1$ for $220 \times 30$ O-grid points and $161 \times 185$ H-grid points in each of the cascades. Thus, the difference in the computated time-averaged parameters of the vortical wake from experimental data remained within the limits of the experimental error.

Figure 17 shows the computed and experimental values of the quantity

$$|\omega_1(\Delta y)| = \left|\frac{\Omega_1(y)}{\Omega_1(y_0)}\right|, \quad \Omega_1(y) = \sum_{m=-20}^{20} \Omega_{1m} e^{i2\pi m \cdot y/h_2}, \quad \Delta y = \frac{y - y_0}{h_2},$$

were $y = y_0$ is the ordinate of the axis of the stationary vortical wake. Distributions were obtained for $\nu = 0{\cdot}2$.

An essential feature of the obtained theoretical and experimental distributions of $|\Omega_1(y)|$ is its non-monotonic variation with increasing distance from the vertical-wake axis. In the flow core, the value $|\Omega_1|$ does not exceed $0{\cdot}1 \times |\Omega_1(y_1)|$. The presented results allow the conclusion that periodic free vortices behind cascade 2 intensively diffuse in zones of stationary vortical wakes of airfoils. Thus, in contrast with diffusion in a uniform flow, with a monotonic

decrease of vorticity with increasing distance from the source, the diffusion of free vortices results in a non-monotonic distribution across a stationary vortical layer.

As one would expect, the nature of the distribution of vorticity as obtained from calculations essentially depends on the number of computational grid points. In particular, the calculations executed for numbers of grid points of the O- and of H-grids, respectively, $100 \times 16, 81 \times 33; 160 \times 26, 121 \times 93$ and $220 \times 30, 160 \times 185$ show that, in the first case, the distribution $|\Omega_1(y)|$ differed considerably from the experimental one over the entire rotor pitch ($0 \le y \le h_2$). For the second and third grid-points values, the difference concerns mainly a part of a local maximum above the vertical-wake axis ($y - y_1 > 0$). It should be noted that this area is located outside the airfoil suction surface of cascade 2 (see Figure 13). It is possible to assume that, in a numerical simulation, the boundary layer on the suction surface of an airfoil is described with insufficient accuracy.

### 5.2. Diffusion of free vortices in turbulent flow

We consider here a semi-empirical model of turbulent diffusion of free vortices that allows us to describe the vorticity distribution obtained in Section 5.1. It is assumed that the velocity of free-vortex shedding is equal to the time-averaged flow velocity in a vortical wake of the airfoil and diffusion, without taking into account the viscosity, occurs because of turbulent pulsations of this velocity across the wake. In other words, free vortices are assumed passive and do not affect the turbulence parameters in a vortical wake. It is possible to expect that a similar model corresponds to real conditions when the frequency of turbulent pulsations considerably exceeds the frequency of free-vortex pulsations.

Let the axis $Ox_1$ of a Cartesian frame of reference $(x_1, y_1)$ be counted from the trailing edge along a stationary vortical wake. The equation of turbulent diffusion of the vorticity $\Omega = \Omega(x_1, y_1, t)$ in the case under consideration has the form

$$\frac{\partial \Omega}{\partial t} + V_0(x_1, y_1)\frac{\partial \Omega}{\partial x_1} = \frac{\partial}{\partial y_1}\left(D \cdot \frac{\partial \Omega}{\partial y_1}\right), \tag{20}$$

where $D$ is the diffusion coefficient, and the velocity of the free-vortices shedding $V_0$ (see, for example, (11)) can be presented according to the self-similar theory of turbulent vortical wakes in the form

$$V_0 = V_1[1 - u_1(x_1, y_1)], \quad u_1 = \frac{\chi}{\sqrt{x_1}}\overline{u}_1(\eta), \quad \eta = y_1/\sqrt{x_1 h_2}, \quad \overline{u}_1(0) = 1.$$

Here $V_1 = \text{const}$ is the velocity in the flow core; $\chi$ is a rather small value ($\sim 0{\cdot}1$) that is uniquely determined by the coefficient of the profile losses. From here Equation (20), in dimensionless form, becomes

$$\frac{1}{q}\frac{\partial \overline{\Omega}}{\partial t} + \frac{\partial \overline{\Omega}}{\partial x} - d\frac{\partial^2 \overline{\Omega}}{\partial y_1^2} = \frac{\chi}{\sqrt{x_1}}\overline{u}_1(\eta)\frac{\partial \overline{\Omega}}{\partial x_1},$$

where

$$d = \frac{D}{V_1 \cdot h_2}, \quad \overline{\Omega} = \frac{\Omega h_2}{V_1}, \quad q = \frac{\omega h_2}{V_1}, \quad \omega = u/h_2. \tag{21}$$

Henceforth the coordinates $x_1, y_1$, and $t$ are assumed to be compared with $h_2$ and $h_2/V_1$, respectively.

The layer of free vortices in the vicinity of the trailing edge of an airfoil is assumed to be a line of contact discontinuity of the velocity, which is determined by Equation (12). From

here the value of the vorticity at point $x_1 = 0$ is given by

$$\Omega(0, y_1, t) = \gamma(0, t) \cdot \delta(y_1) = -\frac{1}{V_1} \frac{\partial \Gamma}{\partial t} \cdot \delta(y_1), \quad \Gamma = \sum_k \Gamma_k \cdot e^{-i2\pi k\omega t}, \tag{22}$$

where $\delta$ is the Dirac's delta-function.

For $\chi = 0$ Equation (21) corresponds to diffusion in a uniform flow with velocity $V_1$. A solution that is periodic in time satisfying the boundary condition (22), as well as the conditions of symmetry over the $y_1$-coordinate and attenuating for $y_1 \to \infty$, results in a distribution of the velocity in a diffusion layer determined by Equation (14), where it is necessary to put $\mathrm{Re} = d^{-1}$. The solution of Equation (21) satisfying the above conditions has the form

$$\begin{aligned}
&\overline{\Omega} = \frac{1}{\sqrt{x_1}} \cdot e^{-\eta^2/4d} \sum_{\substack{k \\ (k \neq 0)}} A_k \cdot \left[ 1 + \frac{\chi}{\sqrt{x_1}} f_1(\eta) + i2\pi kq\chi \sqrt{x_1} f_2(\eta) \right] e^{-i2\pi k(t - qx_1)}, \\
&f_1(\eta) = \frac{\eta}{d} \int_\eta^\infty \frac{1}{\eta_1^2} \cdot e^{\eta^2/4d} \cdot \int_{\eta_1}^\infty \left( \frac{1}{2} - \frac{\eta_2^2}{4d} \right) \eta_2 \overline{u}_1(\eta_2) e^{-\eta_2^2/4d} d\eta_2 d\eta_1, \\
&f_2(\eta) = \frac{1}{d} e^{\eta^2/4d} \int_\eta^\infty e^{-\eta_1^2/4d} \cdot \int_0^{\eta_1} \overline{u}_1(\eta_2) d\eta_2 d\eta_1, \quad A_k = \mathrm{const}
\end{aligned} \tag{23}$$

to within an accuracy determine by $\chi$.

Solution (23) differs significantly from the case $\chi = 0$ in that the whirling fluid particles form a straight line normal to the vortical wake axis at some moment of time and are then bent. Free vortices diffusing in the layers lying at a larger distance from the wake axis are transported at a velocity that exceeds the velocity of vortices located on the axis. For a fixed value of $x_1$ the distribution across a layer of vorticity amplitude depends on the number of the time harmonic $k$. For a fixed value of $y_1$, the amplitude of the vorticity approaches a finite ($\neq 0$) value for increasing $x_1$ and the axial density of the total vorticity across the diffusion layer increases as $\sqrt{x_1}$.

A relation between the coefficients $A_k$ of series (23) and $\Gamma_k (k = 0, \pm 1, \ldots)$ for the expansion of the velocity circulation on an airfoil (see Equation (22)) follows from the condition of preservation of total vorticity in a flow for the entire time of free-vortices formation. For a steady periodic flow (*i.e.*, proceeding for an infinitely long time) this condition gives the relation

$$\lim_{x_1 \to \infty} \frac{d}{dt} [\Gamma(t) + I(x_1, t)] = 0,$$

where

$$I(x_1, t) = \int_0^{x_1} \int_{-\infty}^{\infty} \Omega(x_1, y_1, t) dy_1 dx_1.$$

Upon some algebraic manipulations, we may derive from this:

$$\begin{aligned}
&A_k \left[ 2\sqrt{\pi d} - \chi(1 + i) \sqrt{\frac{\pi}{4\pi kq}} (\Phi_1 - i\pi kq\Phi_2) \right] = 2\pi kqi\overline{\Gamma}_k, \\
&\Phi_1 = \int_{-\infty}^{\infty} e^{-\eta^2/4d} \cdot f_1(\eta) d\eta, \quad \Phi_2 = \int_{-\infty}^{\infty} e^{-\eta^2/4d} \cdot f_2(\eta) d\eta, \\
&\overline{\Gamma}_k = \Gamma_k / h_2 V_1, \quad k = \pm 1, \pm 2, \ldots
\end{aligned} \tag{24}$$

Equation (24) can obviously be used, both for a numerical estimate of the coefficients $A_k$, if the circulation $\Gamma(t)$ on an airfoil is known, and for the determination of the coefficients $\Gamma_k$, if the vorticity $\Omega$ has been measured.

For $\chi = 0$ the coefficient $A_k$ in (24) grows unboundedly when $d \to 0$. In this case, as can be easily concluded from (23), the vorticity $\Omega$ is described by the $\delta$-function; the diffusion layer degenerates to a line of velocity contact discontinuity, and the coefficients $A_k$ are defined by the formula $A_k = 2\pi kq\mathrm{i}\overline{\Gamma}_k$.

In the general case of $\chi \neq 0$, the diffusion-layer width obviously depends on the function $\overline{u_1}$ and, generally speaking, on $d$. Let, for definiteness, the time-averaged velocity in a vortical wake be given by Equation (11). Then

$$\chi = \frac{\sqrt{\zeta^* \cos\alpha}}{1{\cdot}52}, \quad \overline{u}_1 = \begin{cases} \cos^2(\pi k_0 \eta), & |\eta| \le \dfrac{1}{2k_0} \\ 0, & |\eta| > \dfrac{1}{2k_0} \end{cases}, \quad k_0 = \frac{1}{1{\cdot}52\sqrt{\zeta^* \cos\alpha}}, \tag{25}$$

where the parameter $\chi$ defines the wake "depth", and $k_0$ is its half-width corresponding to the condition $|\eta| = 1/2k_0 = \eta_0$. In (23), $f_1(\eta_0) = f_2(\eta_0) = 0$, and the ratio of the vorticity on the boundary of a stationary vortical wake and vorticity on its axis is equal to $\exp(-\eta_0^2/4d)$.

Figure 18 presents results pertaining to the quantity

$$\omega_1(x_1, \eta_1) = \mathfrak{Re}\,\omega_1 + \mathrm{i}\mathfrak{Im}\,\omega_1 = \frac{\Omega_1(x_1, \eta_1)}{\Omega_1(x_1, 0)}, \quad \eta_1 = \frac{2k_0 y_1}{\sqrt{x_1}},$$

where $\Omega_1$ denotes the complex amplitude of the first harmonic in expansion (23), and $\eta_1$ is equal to the distance from the vortical wake axis related to the wake half-width. Calculations were carried out for $\chi = 0{\cdot}131$, and the parameter $d_1 = k_0\sqrt{d}$, as well as the dimensionless distance $x_1$ from the trailing edge of an airfoil along the vortical wake axis, were varied.

As can be seen from Figure 18, the value $\omega_1$ varies non-monotonically across a wake. For a fixed value $k_0$, the diffusion dimensionless coefficient $d$ affects significantly the local extreme in the vicinity of the vortical wake axis.

### 5.3. Comparison with experiment

Detailed measurements of the instantaneous flow velocity behind cascade 2 (see Figure 13) have been conducted for a gap $\Delta_{23} = 23$ mm. Measurement points were placed at distances $x = 6$, 8, 10, 12, 14 and 16 mm from the front exit of cascade 2. The mutual position of cascades 1 and 3 remained fixed ($\nu = 0$), and measurements were carried out for 20 points in regular intervals $h_2$ located on a pitch. While determining the derivative $\partial V_{ykl}/\partial x$ in expansion (19), we used a second-order spline approximation on $x$ points. The Reynolds and Strouhal numbers corresponding to the experimental conditions were equal to $\mathrm{Re} = 6 \times 10^5$, $\mathrm{Sh} = 1{\cdot}17$.

As one would expect, the parameters of the time-averaged vortical wake for the points $x =$ 6 and 16 mm differed appreciably from their values in interval 8 mm $\le x \le$ 14 mm. The coefficient of the profile losses obtained in this interval is equal to $\zeta^* = 0{\cdot}063$, this value was also used for the calculation of the diffusion of free vortices.

Figure 19 shows the results of measurements of value $|\omega_1(x, \Delta y)|$ for sections $x = 8$, 10 and 12 mm. For comparison, the computed results for the diffusion of the first harmonic vorticity and the data obtained for the numerical solution of the Reynolds equations are also presented in Figure 19.

Calculation of the diffusion of free vortices was carried out by Equation (23) for the velocity distribution in the vortical wake as determined by relations (25). In accordance with the experimentally determined coefficient of the profile losses and an exit flow angle $\alpha$, it was concluded that: $\chi = 0{\cdot}131$, $k_0 = 3{\cdot}3$. The calculations that were performed for a dimensionless diffusion coefficient equal to $d = 4 \times 10^{-4}$ show good agreement with experimental data concerning the non-monotonic dependence of $|\omega_1(x, \Delta y)|$ on $\Delta y$. However, the calculated width

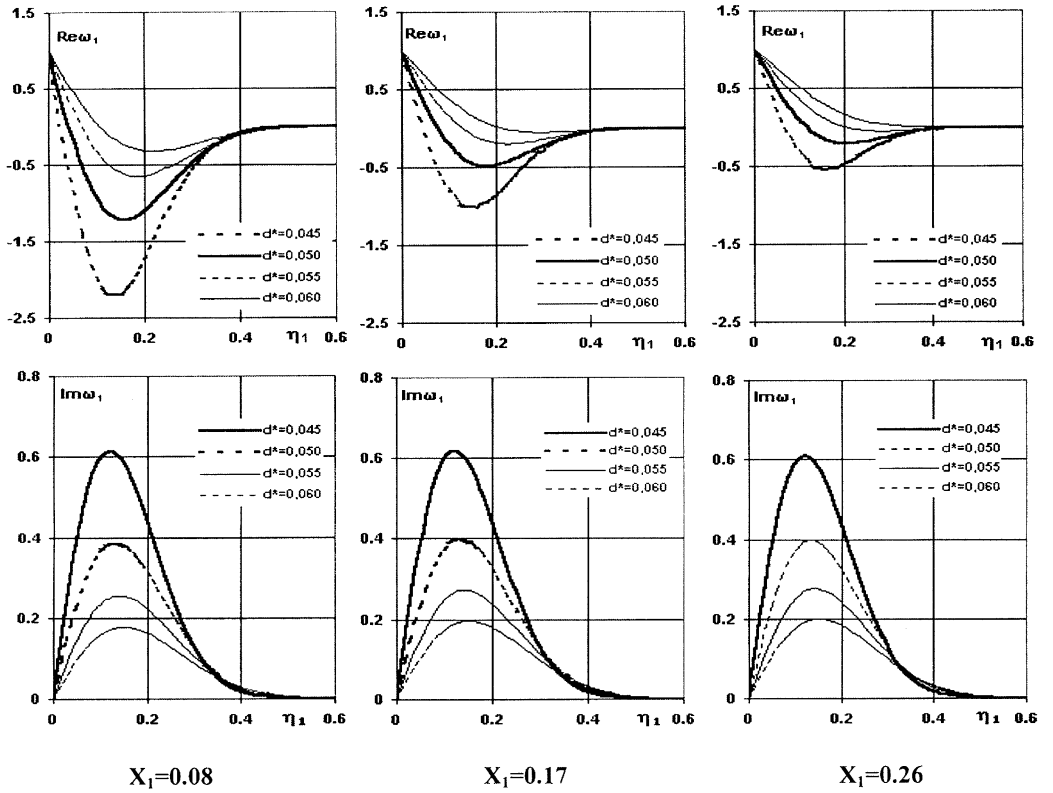


*Figure 18.* Theoretical distribution of the first harmonic amplitude of flow vorticity as a result of free vortices diffusion in the wake of R blade.

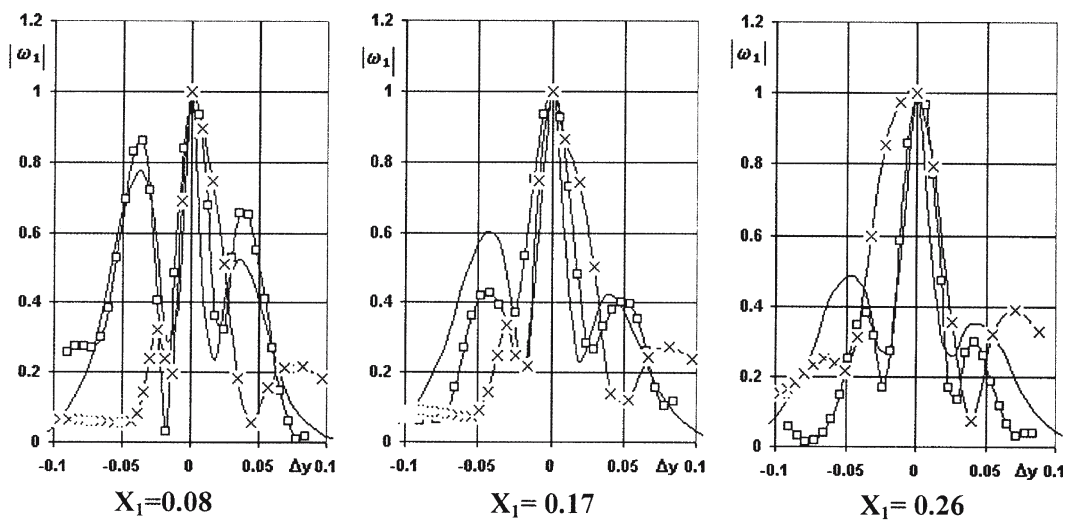


*Figure 19.* Comparison of theoretical and experimental distributions of the first harmonic amplitude of free vortices vorticity in the wake of cascade 2. □ – experiment; x – numerical simulation; — calculation by the theory of diffusion.

of the diffusion layer proved to be 1·5 times less than in our experiments. We assume that this is caused by application of the calculations in the field of measurements closely located to the trailing edges of the airfoils of cascade 2. Actually the character of the formation of free vortices near the trailing edges, where the boundary-layer thickness is significant, can differ from the line-of-contact discontinuity adopted in the theory. According to the specified assumption in the calculations the constant "$b$" has been entered (see (11)). It allows to provide a finite ($\neq 0$) thickness of the diffusion layer in the trailing edge of an airfoil similarly to the theory of a self-similar vortical wake. The calculations presented in Figure 17 were executed for $b = 0{\cdot}13$.

A numerical flow simulation was carried out with $N_1 = N_2 = N_3 = 1$ and a number of O-grid points equal to $160 \times 26$ and $121 \times 93$ H-grid points for each cascade. This provided 93 computational points on a pitch of cascade 2. A further increase in the number of grid points had a little effect on the amplitude of the first harmonic of a circulation pulsation on the airfoils of cascade 2.

Comparison of computational and experimental data allows us to conclude that there is a region of the parameter $d$ for which agreement between the free-vortices diffusion model and measurement is found. The maximum discrepancies between experiment and numerical simulation are observed on a part of the vortical wake on the side of the suction surface of an airfoil of cascade 2. This is also borne out by Figure 17.

## 6. Conclusions

The results of an analytical description of the flow through mutually moving turbomachine cascades proposed in the present paper are summarized here. The complexity of such a description is caused mainly by the fact that, for real gaps between cascades, the problem of their interaction in a flow has no physical meaning without taking into account the vortical wakes behind airfoils. The analytical description of such wakes assumes the use of empirical constants. Corresponding theoretical solutions, which are correct in a mathematical sense, require comparison with experiment. Therefore, much attention has been paid in the present work to such comparisons.

The analytical solutions obtained in the paper are based on the assumption of flow incompressibility. It limits solutions to subsonic flows, but allows the use of a rather advanced theory of boundary-value problems for analytical functions. The efficiency of the algorithm used to obtain the solution is ensured by its representation here as a series expansion in powers of the small parameter $\Delta_0$. This allowed us to reduce the problem in each approximation to an integral equation on an airfoil of one of the cascades. For airfoils of any form, the numerical solution of such equations can be carried out with sufficient accuracy on a personal computer and allows a wide variation of entrance parameters at a small expense of computer time.

It is to be noted that a practical application of numerical methods for the solution of the equations that apply to turbomachines is essentially limited both by a big expense of computing resources and the small number of test results that are due to an insufficient knowledge of the physical properties of similar flows. The experience concerning the application of numerical simulations of hydrodynamic interaction of cascades for the calculation of periodic vortical wakes behind airfoils, as presented in this paper, shows a significant discrepancy with available experimental data, thus necessitating a further improvement of numerical methods. The analytical description of the distribution of periodic vorticity in a vortical wake as proposed here can be useful both for engineering estimates and for comparison with results

of numerical simulation. The obtained results concerning flow properties that were confirmed by experiment consist in the following:

1. In a flow of two mutually moving cascades, the values of the gaps between them determine the hydrodynamic-interaction features. For small gaps potential interaction is dominating. For moderate gaps, which are usually used in practice, the potential-vortical interaction is important. Vortical interaction is typical for large gaps between cascades.
2. Potential-vortical interaction in a flow of three cascades of a stator-rotor-stator type, which is a typical arrangement in cascades in axial turbomachines, has been investigated. It has been found that for multiple airfoils in a total spatial period of the extreme cascades, their mutual shift (clocking) along the front considerably affects the unsteady flow of the middle cascade.
3. It has been shown that the effect indicated in item 2 results in a variation of the pressure pulsations on the airfoils of the middle cascade and, as a consequence of this, in a variation of the radiated noise intensity and total pressure losses in the flow.
4. It has been found that the additional total pressure losses in flows through mutually moving cascades arise owing to dissipation of the free vortices shedding from airfoils.
5. It has been found that the distribution of the vorticity of periodic free vortices in vortical wakes of airfoils is described by their turbulent diffusion in a non-uniform flow (Table 2).

*Table 2.* Nomenclature

| | |
|---|---|
| $D$ | turbulent diffusion coefficient |
| $H = N_\mu h_\mu (\mu = 1, 2)$ | common period of two cascades of airfoils |
| $h_\mu (\mu = 1, 2)$ | pitch of the $\mu$th cascade of airfoils |
| $J$ | perturbation of complex conjugate flow velocity in stationary vortex wakes of cascades of airfoils |
| $J_\mu (\mu = 1, 2)$ | perturbation of complex conjugate flow velocity caused by free vortices behind the airfoils of the $\mu$th cascade |
| $L$ | sound intensity |
| $L_{\mu m} (\mu = 1, 2; m = 0, \pm 1, \ldots)$ | airfoil of the $\mu$th cascade with number $m$ |
| $N_\mu (\mu = 1, 2)$ | number of airfoils of the $\mu$th cascade in the common circumferential period of two cascades |
| $P$ | static pressure |
| Re | Reynolds Number |
| $r$ | radial coordinate of a point |
| $s, \sigma$ | arc coordinates of points on the original cascade airfoil, which are measured from the outlet edge in positive direction of airfoil tracing (in counter-clockwise manner) |
| Sh, $q$ | Strouhal Number |
| $T, T_0$ | time periods in the frames of reference of rotor and stator, respectively |
| $t$ | time |
| $u$ | linear velocity of motion of a moving cascade of airfoils |
| $V$ | potential part of complex conjugate flow velocity |
| $V_\Sigma$ | complex conjugate flow velocity in cascades of airfoils |
| $V_\infty$ | complex conjugate flow velocity at an infinite upstream distance from the cascade of airfoils |
| $x$ | axial coordinate of a point |
| $y, y_0$ | coordinates of a point measured along the front of the cascade of airfoils |
| $z, \zeta$ | complex coordinates of points in the plane of the cascade of airfoils |

| | |
|---|---|
| $\Delta$ | gap between two cascades |
| $\Delta_{12}, \Delta_{23}$ | gaps between the cascades 1–2 and 2–3 in the set of cascades 1–2–3 |
| $\Delta\varphi, \Delta\varphi_0$ | angular pitches between the rotor and stator blades, respectively |
| $\Gamma_{\mu m}(\mu = 1, 2; m = 0, \pm 1, \pm 2, \ldots)$ | circulation of flow velocity on the $m$th airfoil of the $\mu$th cascade |
| $\varphi, \varphi_0$ | angular coordinates of a point |
| $\nu$ | relative shift along the front of cascades 1 and 3 in the set of cascades 1–2–3 |
| $\Omega$ | flow vorticity caused by turbulent diffusion of free vortices behind the cascade airfoil |
| $\Omega_0$ | angular velocity of rotor rotation |
| $\zeta^*$ | empirical factor of profile losses |

## References


1. V.E. Saren, On hydrodynamic interaction between profile cascades in a potential flow. *Izv. Acad. Nauk SSSR, Mekhanika Zhidkosti i Gasa* 4 (1971) 75–84 (in Russian).
2. V.A. Yudin, Calculation of hydrodynamic interaction of profile cascades with effect of wing wake. *Aeroelasticity of Turbomachinery Blades*, Trudy CIAM, No. 953, Moscow: Central institute of aviation motors (1981) pp. 52–56 (in Russian).
3. V.E. Saren and V.A. Yudin, Influence of axial clearance on hydrodynamic interaction of profile cascades. *Aeroelasticity of Turbomachine*, Novosibirsk: Institute of Hydrodynamics (1984) pp. 33–42 (in Russian).
4. V.A. Yudin, Calculation of hydrodynamic interaction of profile cascades with effect of unsteady wing wake diffusion. *J. Appl. Mech. Techn. Phys.* 42 (5) (2001) 61–69 (in Russian).
5. V.E. Saren, Some ways of reducing unsteady load due to blade rows hydrodynamic interaction in axial flow turbomachine. *Trans. of 2nd Intern. Conf. on Engineering Aero-Hydroelasticity*. Pilsen–Czech Republic (1994) pp. 160–165.
6. V.E. Saren, Relative position of two rows of axial turbomachine effect on aerodynamics in a row placed between them. *Unsteady Aerodynamics and Aeroelasticity of Turbomachines*. Amsterdam: Elsevier (1995) pp. 421–425.
7. F.W. Huber, P.D. Johnson, O.P. Sharma, *et al.*, Performance improvement through indexing of turbine airfoils. Part 1. Experimental Investigation. *ASME Paper* GT-27 (1995).
8. L.W. Griffin, F.W. Huber and O.P. Sharma, Performance improvement through indexing of turbine airfoils. Part 2. Numerical Simulation. *ASME Paper* GT-28 (1995).
9. D.J. Dorney and O.P. Sharma, A study of turbine performance increases through airfoil clocking. *AIAA Paper* 2816 (1996).
10. V.E. Saren, N.M. Savin, D.J. Dorney and R.M. Zacharias, Experimental and numerical investigation of unsteady rotor-stator interaction on axial compressor stage (with IGV) performance. *Unsteady Aerodynamics and Aeroelasticity of Turbomachines*. Dordrecht: Kluwer (1998) pp. 407–416.
11. V.E. Saren, N.M. Savin, D.J. Dorney and D.L. Sondak, Experimental and numerical investigation of airfoil clocking and inter-blade-row gap effects on axial compressor performance. *Int. J. Turbo Jet Engines* 15 (1998) 235–252.
12. D.J. Dorney, D.L. Sondak, P.G.A. Cizmas, V.E. Saren and N.M. Savin, Full-annulus simulations of airfoil clocking in a 1-1/2 stage axial compressor. *Int. J. Turbo Jet Engines* 16 (1999) 149–160.
13. N.M. Savin and V.E. Saren, Hydrodynamic interaction of the blade rows in the stator-rotor-stator system of an axial turbomachine. *Fluid Dyn.* 35 (2000) 432–441.
14. W. Hohn, Numerical and experimental investigation of unsteady flow interaction in a low pressure multistage turbine. *Proc. 15th Int. Symp. on Airbreathing Engines*, Bangalore, India No. 2001-1199 (2001).
15. J. Krysinski, J. Blaszczak and A. Smolny, Two-stage turbine experimental investigations of unsteady stator-stator interaction (indexing effect). *Proc. 10th Int. Symp. on Unsteady Aerodynamics, Aeroacoustics and Aeroelasticity of Turbomachines*. Durham, North Carolina, USA (2003).
16. V.E. Saren, N.M. Savin and V.G. Grupa, Experimental and computational research of a flow structure in a stator-rotor-stator system of an axial compressor. *Unsteady Aerodynamics, Aeroacoustics and Aeroelasticity of Turbomachines*. Lyon, France: Fluorem (2001) pp. 494–502.
17. N.M. Savin and V.E. Saren, Stator clocking effect in a system of rows stator-rotor-stator of the subsonic axial compressor. *Proc. 10th Int. Symp. on Unsteady Aerodynamics, Aeroacoustics and Aeroelasticity of Turbomachines*. Durham, North Carolina, USA (2003).

18. V.E. Saren and S.A. Smirnov, Unsteady vortical wakes behind mutually moving rows of axial turbomachine. *Thermophys. Aeromech.* 10 (2003) 175–188.
19. G.Ju. Stepanov, *Hydrodynamics of Turbomachinery Cascades*. Moscow: Fizmatgiz, (1962) 512 pp. (in Russian).
20. G.S. Samoilovitch, *Turbomachine Blades Vibration Excitation*. Moscow: Maschinostroenie (1975) 287 pp. (in Russian).
21. V.P. Rjabchenko and V.E. Saren, To aerodynamic characteristics calculation of arbitrary form profile cascades. *Izv. Acad. Nauk SSSR, Mekhanika Zhidkosti I Gaza* 2 (1972) 105–112 (in Russian).
22. V.A. Yudin, Profiles cascade in unsteady vortical flow. *J. Appl. Mech. Techn. Phys.* 35 (4) (1994) 85–91 (in Russian).
23. T. Adachi, K. Fukusado, N. Takanashi and Y. Nakamoto, Study of the interference between moving and stationary blade rows in axial flow blower. *Bull. JSME* 17, 109 (1974) 904–911.
24. F.J. Heymann, Turbine blade vibration due to nozzle wakes. *J. Engng. Power* 91 series A 4 (1969) 1–20.
25. M.Ya. Ivanov, V.G. Krupa and R.Z. Nigmatullin, Implicit high order accuracy Godunov type scheme for integration of Navier-Stokes equations. *J. Comp. Math. Math. Phys*. 29 (1989) 888–901.
26. T.J. Coakley, Turbulence modeling methods for the compressible Navier-Stokes Equations. *AIAA Paper* 83-1693 (1983).
27. M.M. Rai, A relaxation approach to patched-grid calculations with the Euler equations. *AIAA Paper* 85-0295 (1985).
28. D.V. Kovalev, V.E. Saren and R.A. Shipov, Influence of mutual stators circumferential shift upon the noise generated by stator-rotor-stator blade-row system in the axial-flow compressor. *Proc. 10th Int. Symp. on Unsteady Aerodynamics, Aeroacoustics and Aeroelasticity of Turbomachines*, Durham, North Carolina, USA (2003).